FY 2020 2nd Quarter Research Performance Progress Report

Project Title:	Basin-specific geochemistry to promote unconventional efficiency
Project Period:	10/01/18-9/30/21
Reporting Period:	01/01/20-03/31/20
Submission Date:	4/30/2020
Recipient:	SLAC National Accelerator Laboratory
Recipient DUNS #:	92-9824415
Address:	2575 Sand Hill Road, MS 69
	Menlo Park, CA 94025
Website (if available)	www-ssrl.slac.stanford.edu
Award Number:	FWP 100211
Awarding Agency:	DOE/NETL

Principal Investigator:	John R. Bargar
	Senior Staff Scientist
	SLAC National Accelerator Laboratory
	Phone: 650-926-4949
	Email: bargar@slac.stanford.edu
Co-Principal Investigators:	Adam Jew (SLAC National Accelerator Laboratory)
	Katharine Maher (Stanford University)
	Anthony Kovscek (Stanford University)
	Tiziana Vanorio (Stanford University)
	Gordon E. Brown, Jr. (Stanford University and SLAC National Accelerator Laboratory)
NETL Project Manager:	Olayinka Ogunsola
	Elena Melchert
	David Cercone

Table of Contents

Abbreviations

Ba	=	Barium
CT	=	Computed tomography
D	=	Darcy (unit)
Da	=	Damköhler number
DDI	=	Double de-ionized water
DGSA	=	Distance-based generalized sensitivity analysis
DM	=	Drilling mud
DO	=	Dissolved oxygen
DOE-FE	=	Department of Energy – Fossil Energy
EDS	=	Energy dispersion spectroscopy
EGSP	=	Eastern Gas Shales Project
Fe	=	Iron
FOV	=	Field of view
FWP	=	Field work plan
FY	=	Fiscal Year
GTI	=	Gas Technology Institute
HCl	=	Hydrochloric acid
H_2SO_4	=	Sulfuric acid
HFF	=	Hydraulic fracturing fluid
HFTS	=	Hydraulic fracturing test site
I.S.	=	Ionic strength
KM	=	Knowledge Management
Kr	=	Krypton
LBNL	=	Lawrence Berkeley National Laboratory
LLNL	=	Lawrence Livermore National Laboratory
MIP	=	Mercury intrusion porosimetry
MSEEL	=	Marcellus Shale Energy and Environment Laboratory
MXL I/S	=	Mixed-layer illite-smectite
NETL	=	National Energy Technology Laboratory
New Mexico BG	=	New Mexico Bureau of Geology
Pe	=	Péclet number
ppm	=	parts per million (unit)
S	=	Sulfur
SANS	=	Small angle neutron scattering
SEG	=	Society of Economic Geologists
SEM	=	Scanning electron microscopy
SIE	=	Synthetic invert emulsion
Sr	=	Strontium
SRA	=	Source rock analysis
SRV	=	Simulated rock volume
SSRL	=	Stanford Synchrotron Radiation Lightsource
Texas BEG	=	Texas Bureau of Economic Geology
TOC	=	Total organic carbon
µ-XANES	=	Micro-X-ray absorption near-edge spectroscopy
URTeC	=	Unconventional Resources Technology Conference
XAS	=	X-ray absorption spectroscopy
XRF	=	X-ray fluorescence
XRD	=	X-ray diffraction

Motivation and Priority Research Needs

Fluid-shale reactions begin within seconds of injecting hydraulic fluids into unconventional reservoirs (**Figure 1**) and continue throughout shut-in and production, altering and weakening shale fracture surfaces and precipitating mineral scale. These secondary minerals frustrate attempts to recycle produced water, clog pore spaces, and inhibit escape of hydrocarbons from the resource-rich matrix. On the other hand, if we can understand and mitigate these processes, and we can provide this information to industry in the form of easily-implementable and incremental technical solutions, then we can help to improve safe and sustainable water reuse and enhance the efficiency of unconventional gas and oil production on a massive scale. Addressing these challenges strengthens U.S. energy, water, environmental, and economic security.[1] Here we focus on two strategic geochemistry-based research thrusts that will provide new knowledge in the following areas that can be used immediately by industry to improve hydrocarbon recovery: *(i)* mitigating scale precipitation in shale reservoirs; and *(ii)* improving extraction of hydrocarbons from tight matrix pore space (**Figure 2**). Additionally, we are developing a new acoustic monitoring approach that will eventually provide a way to nondestructively monitor shale alteration *in-situ* in the laboratory and subsurface.

Our industry collaborations and our previous DOE-FE-funded research have shown that unconventional oil and natural gas stimulation practices create conditions favorable for scale formation that permanently attenuate permeability and can reduce production.[2-5] Moreover, scale precipitation will intensify when operators inject reused saline water rich in dissolved solutes that can precipitate as secondary minerals, a practice that is increasing rapidly in major producing regions such as the Midland Basin. Chemical scale inhibitors designed to slow the rate of secondary mineral precipitation are largely ineffective in unconventional systems,[4, 6-8] because shut-in times far exceed the inhibition delay. Moreover, organic additives and natural organic compounds dramatically increase iron scale precipitation.[2] Thus, scale precipitation in unconventional systems remains largely unsolved and poorly understood. This project directly addresses these problems.

Basin-specific approach. This project adopts a basin-specific approach in which the fracture fluid compositions and injection schedules unique to a given shale play impact fluid-mineral and fluid-organic reactions occurring within a given basin. We will initially focus on two major unconventional basins, Marcellus (Appalachian) and Permian (West Texas), due to their economic importance and contrasting petrochemical factors (natural gas vs. oil wells) and differing complexity of fracture stimulation fluid compositions (< 10 additives for

Vision. We are on the verge of being able to use shale-fluid reaction geochemistry to solve targeted long-standing challenges in unconventional hydrocarbon production. Doing so will require that we can address three critical needs: (i) Developing predictive knowledge of geochemical reactions occurring in unconventional reservoirs when they are stimulated with water-based fluids; (ii) Identifying specific stimulation steps that enhance mineral scale formation and attenuate production, and then mitigating these problems by modifying stimulation practices through *incremental* changes that can be embraced by operators and producers; and (iii) Using this new knowledge to surgically promote the formation and connection of microscale porosity across shale-fluid interfaces to improve our ability to access hydrocarbons in matrix that are currently unreachable.

We envision that iterative experimentation, microscale observation, modeling, and development/application of novel approaches will allow us to use shale geochemistry to transform fracture stimulation. Further, by working with engaged industry partners, we will be able to provide technical solutions compatible with industry expertise.

Marcellus shale vs. >15 additives for Permian basin). Variations in pH and I.S. will be used to mimic different portions of the SRV, from those near the borehole to distal (**Figure 1**).

Goals

This project is conducting fundamental and applied R&D in four interrelated activities (Tasks 2.1, 2.2, 2.3, and Task 3, below) with the goals of: (i) identifying stimulation practices that promote mineral scale formation, and then, (ii) developing solutions to reduce or eliminate these problems by *incrementally* modifying stimulation practices in ways that can be embraced by operators and producers. Through interactions with industry collaborators and representatives, we are also (iii) promoting new best-practices based on geochemical insights from this DOE-FE-sponsored research.

The four interrelated tasks we are undertaking to achieve these goals are as follows:

Task 2.1. *Understanding the chemical parameters/reactions related to individual basins using a basin-specific approach with their respective shales and various HFF recipes*

Task 2.2. *Mitigating mineral scale formation by developing new chemical formulations derived from experimental results and thermodynamic/kinetic modeling*

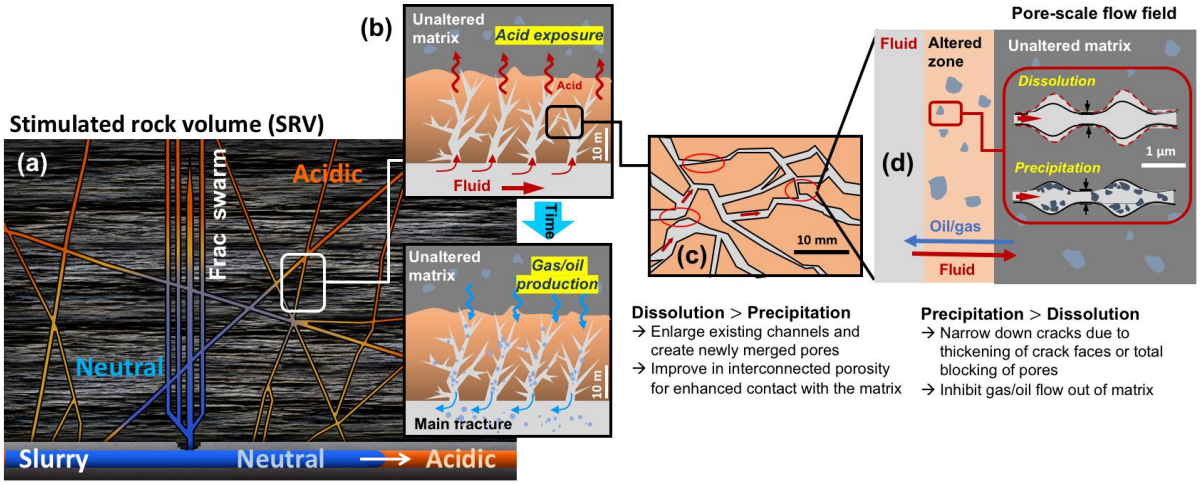

Figure 1. *Schematic of fracture system across length scales.* ***(a)****: During stimulation, the highly acidic spearhead, which is the first injection step, attacks rock and drilling mud in the vicinity of the well bore, releasing barium and sulfate from the mud. Subsequent pad and slurry injections push acid outward towards the periphery of the stimulated rock volume (SRV). During shut-in, acid remains in the peripheral fracture network, whereas the environment near the well bore is at near-neutral or alkaline pH (≥7), i.e., typical of pad and slurry fluids. Barium leached from drilling mud is transported out into the fracture network along with other dissolved minerals that are present in the make-up water (in the case of brine or recycled flowback) that was used for the fracture fluids.* ***(b)*** *During shut-in, the fracture fluid leaks-off (is imbibed or diffuses) into the shale matrix, leading to uncontrolled alteration of the matrix. In the peripheral zone of the SRV, prolonged, uncontrolled acid attack initially creates porosity, which subsequently fills with secondary scale minerals. In all locations, barium and other dissolved minerals transported by the injected fluids precipitate as barite and other types of mineral scale on fracture surfaces and within matrix. Mineral scale precipitation clogs flow paths, slowing or preventing hydrocarbons from escaping matrix.* ***(c).*** *Dissolution, if controlled, can enhance production by increasing apertures of microfractures and pore space* ***(d)****.*

In these activities, we will create knowledge about scale precipitation from a basin-specific research program, and then apply it to mitigating this problem. Thermodynamic and kinetic modeling of the chemical reactions will be used to rapidly assess a large range of chemical parameters, reducing experimental time and waste.

Task 2.3. *Developing a new in-situ method for monitoring secondary porosity and mineral scale generation in the field using acoustic methods*

Due to the high prevalence of mineral scale in shale systems, a new method is needed for determining secondary porosity generation and mineral scale formation in the field. This task will study changes in P- and S-wave velocities in shales reacted with fracture fluid and will identify pore-scale processes that result in alteration of rock permeability (mineral dissolution/scale formation). Laboratory experiments will evaluate the effectiveness of this method and will build a library of data that ultimately can be scaled up for field implementation.

Task 3. *Tailor the altered zone for optimal solution/gas transport through chemical manipulation of the system*

Fluid and gas exchange into/out of the shale matrix is strongly enhanced by secondary porosity created by acidification and pre-existing micro-fractures. Our recent results indicate that permeability of the altered zone (**Figure 1**) can be maintained and improved as long as mineral dissolution and scale precipitation occur concurrently in a controlled fashion. This task will perform research to determine how to tailor the altered zone to enhance dissolution/precipitation rates.

Table 1. Synopsis of tasks

Task 1	Project management
Task 2	Scale prediction and mitigation in stimulated rock volume
2.1	**Prediction of mineral scaling in unconventional reservoirs**
2.1.1	Experimental task
2.1.2	Modeling task
2.2	**Mitigation of mineral scaling in unconventional reservoirs**
2.2.1	Modeling task
2.2.2	Experimental task
2.3	**Acoustic measurements on laboratory-reacted shales**
Task 3	**Manipulation of matrix accessibility**
3.1	Manipulate rates of mineral dissolution and precipitation
3.2	Growth and connectivity of secondary porosity
3.3	Modeling subtask
3.4	Predict and test optimal conditions

Overview of activities and results in FY 2020 Q2

Task 2.1.1. Prediction of mineral scaling in unconventional reservoirs. Experimental: Experiments using basin-specific recipes with their corresponding rocks for two out of three basins (Delaware Basin and Marcellus) have been completed as well as nearly all the characterization analyses. Wolfcamp core was received earlier in the quarter and the samples were prepared for experimentation prior to facility shutdown due to Covid-19. The two analysis areas that still need to be completed on Bone Spring (Delaware Basin) and MSEEL (Marcellus) are imaging (CT and SEM) and permeability. Imaging issues was due to either machine maintenance or moving of equipment between buildings at Stanford and we are still waiting on delivery of the permeability analyzer.

Important results pertaining to Bone Spring samples show that despite being relatively impermeable (< 5 nD), HFF was able to penetrate the Bone Spring shale and react with the Fe-bearing phases. This is primarily due to mineral dissolution of the rock caused by the HCl spearhead allowing fluid penetration into the rock. Synchrotron-based X-ray fluorescence mapping coupled with X-ray absorption spectroscopy (both bulk and micro-) showed that almost all the iron had been oxidized to Fe(III). These results demonstrate the importance of the acid spearhead and subsequent formulation in order to move the HFF into the rock. These results also improve our understanding of the geochemical reactions occurring in shale reservoirs during fracture stimulation.

Task 2.1.2. Prediction of mineral scaling in unconventional reservoirs. Modeling: In **FY2020 Q2**, we completed the development of the workflow for global sensitivity analysis of our reactive transport model. Initial analysis results were obtained for pH, porosity, $Fe(OH)_3$ formation, and barite formation at Day 21 of shale-fluid reaction. In general, pH and reaction rates, as well as some of the factors that affect pH and reaction rates, are the most important, but not all factors affecting the pH and reaction rates are on the list. We will continue analyzing the results we obtained from global sensitivity analysis. Next, we will conduct local sensitivity analysis to better understand the most important parameters during shale-fluid interactions.

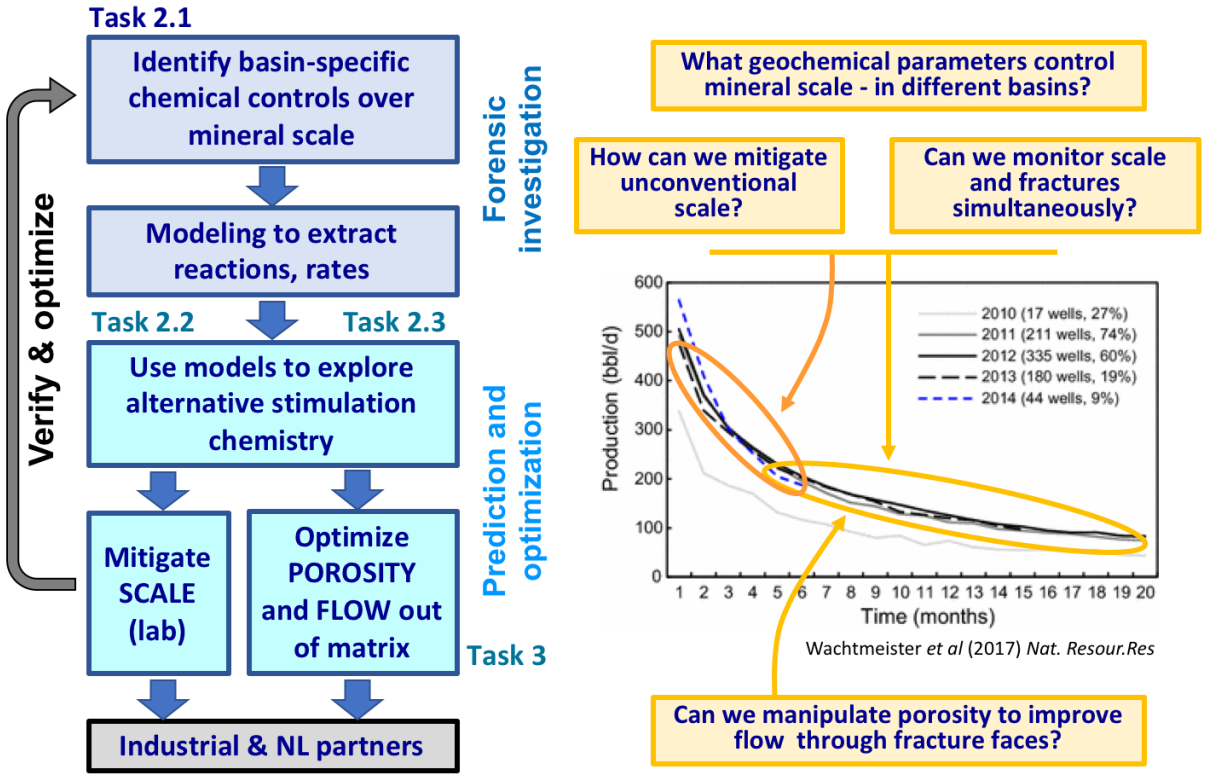

***Figure 2**. Diagrammatic representation of overall project and connection to broader context.*

Task 2.2 Mitigation of mineral scaling in unconventional reservoirs. A new pathway for mitigating Sr scaling in the Permian Basin was devised that does not include the use of anti-scalants in the injection fluid. Our vision is that, by treating the clean brine in the holding ponds at the surface for Sr removal, it should be possible to reuse saline water for injections to limit the amount of waste water produced and lower the strain on the local freshwater sources.

Experiments were performed using $CaSO_4$ minerals in order to initate one of these, or a combination of these, desired Sr-removing processes: 1) Sr adsorption, 2) Sr incorporation, 3) $SrSO_4$ epitaxial growth over $CaSO_4$ crystals. Due to the Covid-19 shutdown, the solution and solid samples have not been analyzed to determine the efficacy of the treatments.

Task 2.3. Acoustic measurements on laboratory-reacted shales: Geochemical fracture alteration of the clay-rich MSEEL sample was simulated by reacting an artificial fracture with hydrochloric acid, which

produced altered zones adjacent to the fracture clearly visible in micro-CT images. While P- and fast S-wave velocities were unaffected by the geochemical alteration, slow S-wave velocities showed measurable reduction and therefore could be a useful monitoring tool.

Task 3. Manipulation of matrix accessibility: The manuscript on reactive flow experiments of clay-rich Marcellus outcrop and carbonate-rich MSEEL shales was prepared and submitted for the SPE WRM. SEM-EDS tools were utilized to explore the predominant reasons for the reduction in porosity and permeability of reacted carbonate-rich MSEEL sample. Imaging results indicate significant barite scale growth due to the reaction between formation water, the fracture fluid, and/or the core sample. The overall decrease in CT-values within cross sectional images after reaction indicates extensive dissolution of calcite-rich sample regions especially in the injection side of the core sample similar to the "altered zone" between the matrix and main fractures. Compaction of the dissolved core sample under confining stress and pore-filling by Al and Mg hydroxide precipitates explain much of the reduction in porosity.

Impact of COVID-19 crisis and our response: Our laboratory operations were halted on Mar 15, 2020 in response to the growing COVID-19 crisis under order from the director of SLAC and (separately) from the health officer of the county of San Mateo. The cessation of laboratory operations has provided an opportunity to write manuscripts, work on modeling, analyze data collected in Q1 and Q2, and plan future measurements. Everyone in the group has been busy with this work. We will continue in this mode in Q3 until work restrictions are lifted.

Based on currently available information from SLAC (which is being updated weekly), we estimate that our laboratories will be closed for ≥ 4 months, opening again for operations in July. Starting from the time laboratories reopen, we expect an additional delay of two months to perform standard chemical analyses on samples already generated (but not yet analyzed), due to the large backlog and high demand by all users of the shared analytical facilities. All scheduled beam time was canceled at the Stanford Synchrotron Radiation Lightsource after Mar 15, it will be rescheduled after work restrictions are lifted. SLAC has announced that it will take a slow and deliberate path to restarting beam lines, and that the total number of visiting scientists will be maintained at low levels. Accordingly, we are anticipating that an additional 4 to 6 months of delay will be introduced following the restart of laboratory operations in order to complete outstanding synchrotron characterization measurements. We have made an initial forecast of revised milestone completion times in the MILESTONE STATUS section.

Synergies with other national laboratories

We collaborate extensively and frequently with NETL and LBNL to accomplish DOE-FE research mission needs through a twice-monthly ad-hoc shale geochemistry teleconference meeting/seminar series. This is an inclusive meeting, meant to foster collaborative interactions and accelerate discovery within the fundamental shale geochemistry research community. All interested parties from universities and other labs are welcome to participate and do so frequently. We are also collaborating extensively with LBNL, LLNL, and NETL in the DOE-FE funded HFTS multiscale research program. We have recently begun to discuss synergistic collaboration opportunities with the LANL shale geochemistry team.

Collaboration and interactions with other national laboratory programs. Multiple teleconferences and in-person meetings have been held each month since the start of the fiscal year with research scientists at NETL (A. Hakala, C. Lopano, M. Stuckman, B. McAdams, and W. Xiong), LLNL (J. Morris) and LBNL (H. Deng, T. Kneafsey, M. Reagan, and C. Steefel) to support the ongoing research program. On Dec. 18. 2019, we conducted a SLAC-NETL-LBNL HFTS planning meeting.

The SLAC geochemistry team is performing synergistic activities that provide unique and valuable services to the other DOE-FE research programs. Our team has deep expertise in the area of fracture fluid

formulations. After expending a significant effort developing basin-specific stimulation fluid recipes for Marcellus, Midland, and Delaware basins for our research activities, we shared these recipes with collaborators at NETL, LBNL, and LLNL to help ensure that the larger DOE-FE shale research portfolio can benefit from our efforts and to be able to more readily compare experimental results from different national labs. Other key services provided recently include: (*i*) Providing new research results and data to partner labs through ad-hoc collaborations and through the formal HFTS program (*e.g.*, as documented in the HFTS project quarterly and annual reports); (*ii*) Collecting Bone Spring formation shale samples from the field and providing them to NETL and LBNL collaborators; (*iii*) Helping other projects to collect synchrotron data; (*iv*) Participating in the Knowledge Management (KM) meeting group (Jew); and (*v*) Regularly contributing questions and discussions to the KM discussion form.

Schedule for collaborative interactions. We are participating in the following standing meetings: (*i*) twice-monthly SLAC-NETL-LBNL fundamental shale geochemistry meeting/ seminar series; and (*ii*) twice-monthly HFTS leadership group meetings. The SLAC team participated in two all-day HFTS project planning meetings in Berkeley, CA on Jan 15 and 16, 2020, where we engaged with research teams at NETL, LBNL and LLNL.

Other Collaborative Leveraging. Our collaborations with Pioneer Natural Resources and Equinor North America are providing invaluable insights into industrial fracture stimulation injection chemistry, fluid and additive sequencing, volumes, and rates that are critical in order to understand what operators are doing in highly complex unconventional oils systems. We are also collaborating with the Stanford University EFRC project led by T. Kovscek. Imaging methods developed in the EFRC project will eventually be applied to the applied NETL R&D program.

Details of task progress

Task 1: Project Management
J. Bargar, SLAC

Outreach to industry and academia. J. Bargar participated as a reviewer for the upcoming **URTeC 2020** sub-theme, “Oil/Gas/Water: Fluid-Fluid, Fluid-Rock Interactions & Chemostratigraphy”. Bargar and Jew will participate as co-chairs for the same session at the URTeC 2020 conference in Denver, CO on July 20-22, 2020. Bargar co-organized a symposium on unconventional stimulation geochemistry, entitled, “Environmental Challenges and Solutions in Oil & Gas Development”, to be held at the **259th ACS National Meeting and Exposition** in Philadelphia, PA on Mar 22-23, 2020.

Task 2: Scale prediction and mitigation in the stimulated rock volume

Task 2.1: Prediction of mineral scaling in unconventional reservoirs

Task 2.1.1: Experimental activity

E. Spielman-Sun, SLAC

Objectives and Approach

The primary objective for this task is to understand geochemical processes that control mineral scaling when basin-specific chemical formulations are used for the fracture stimulation fluids. By using region-specific chemical formulations, we aim to understand the formation of primary mineral scale and the

major chemical reactions/parameters that are required for precipitation of mineral scale. By understanding these chemical principles (in Task 2.1), we should be able to predict (in Task 2.2) the impact of new formulations on scale precipitation in specific shale plays, including anticipating and mitigating mineral scaling problems that are likely to occur as new formations/plays are opened up for exploration.

Our previous work has shown the importance of fracture fluid and organics native to unconventional systems on the formation of mineral scale.[2, 3, 5, 9] Though this body of work has resulted in several important discoveries, the fluid compositions used were specific to the Marcellus region. A detailed investigation of the number of chemicals used in stimulations for various regions shows that there is a wide variety of major additive chemicals (biocides, breakers, surfactants, etc.) used in a given region. These differences necessitate a basin-specific approach in which the fracture fluid recipe for a given region is used for the corresponding shale type. This basin-specific approach will focus on Marcellus and Midland plays since they are different in mineralogy, targeted hydrocarbon (natural gas vs. oil), and fluid recipe.

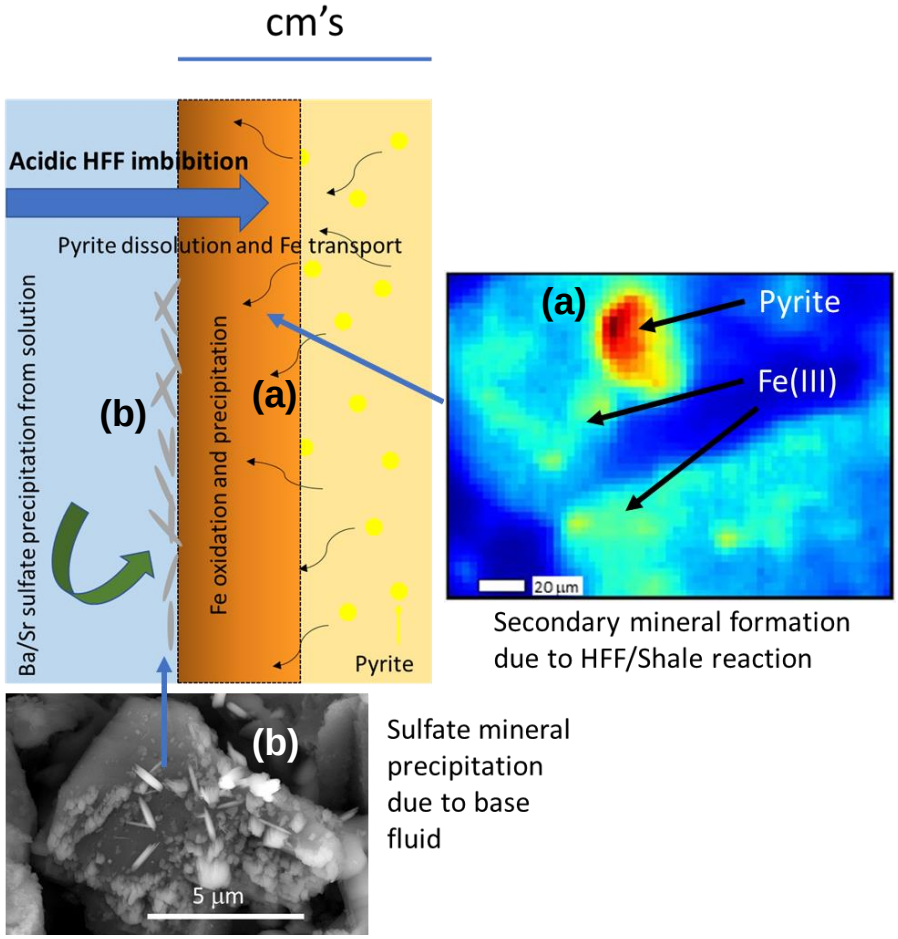

Figure 3. *Conceptual model of mineral scale formation along a fracture. Mineral precipitation inside of the shale matrix (**a**) is primarily in the form of Fe(III) due to pyrite partial dissolution and Fe oxidation caused by fracture fluid. (**b**) Sulfate mineral precipitation on the surface is derived by injection fluids transporting Sr, Ba, SO_4, etc. to the surface allowing for precipitation from the surface inwards. This processes create two mineral scaling fronts moving in opposite directions that build towards each other (inside/out, Fe(III) scale and outside/in, SO_4 scale).*

Previous experiments also did not consider the injection sequence of a typical stimulation. Rather, all of the chemicals were mixed together prior to reaction with the shale. To better simulate real-world systems, the new experiments follow the sequential addition of chemicals based on the injection schedules procured for the different shale plays. Not only will this sequential addition result in significant changes to additive concentrations at different times of the experimental process, but the different times between various stages allows varying pH's to interact with the shale depending on the dilution of the acid caused by subsequent solution additions. This sequential addition also allows for adjusting of the system in order to mimic different regions of the system (proximal to the well bore, distal to the well bore, and in-between), in which each region will have different pH conditions.

A final consideration is the base fluid used for injection. We know that fracture fluid chemicals will alter the shale matrix. Minerals such as pyrite will partially dissolve and the released Fe will oxidize and precipitate, an inside-out mineral scaling. On the other hand, our previous work with Ba-laden drilling mud and our work with Pioneer have also shown the importance of mineral scaling on the surface due to the injected fluid containing the components for mineral precipitation, an outside-in mineral scaling (**Figure 3**).

Table 2 *Task 2.1.1 Objectives for FY2020 Q2*

Goal	Status
Characterize Bone Spring and Marcellus post-reaction ground shale, laboratory methods	Complete
Synchrotron-based characterization of Bone Spring and Marcellus post-reaction ground shale: XRF maps	Complete
Synchrotron-based characterization of Bone Spring and Marcellus post-reaction ground shale: bulk Fe and S XAS	Ongoing
Characterize Bone Spring and Marcellus post-reaction whole shale cores	Ongoing
Reaction of Wolfcamp samples with fracture fluids	Scheduled

Progress in FY 2020 Quarter 2

Using previously determined basin-specific fracture fluid recipes and injection schedules (**Appendices B and C**), Bone Spring (Delaware basin; top and bottom units) and Marcellus shale (MSEEL site; outcrop sample from Oatka Creek, Le Roy NY) samples were exposed to synthetic fracture fluids. Characterization of the unreacted core (1" diameter x 1" length) and ground (150-250 µm) samples were discussed in previous reports (Bone Spring, **Quarter 3 Report, 2019**; Marcellus, **Quarter 4 Report, 2019**). One subset of ground samples was reacted in glass serum bottles, herein referred to as "Time-Resolved Reactors", to allow sampling of solution every 72 hours to evaluate solute evolution with time. Solution analyses for Bone Spring and Marcellus were previously discussed (**Quarter 1 Report, 2020**).

In Quarter 2, the rest of the samples (ground and cores) were pressurized to 85 bar and reacted for a total of 3-weeks at 80°C, herein referred to as "Pressurized Reactors" after which solution samples were collected and solid samples were rinsed with doubly de-ionized water (DDI) and dried for further analysis. Reactor experiments were performed in duplicate to account for shale heterogeneity. Lab-based characterization and analysis of these ground precipitates is complete and results discussed below in this report. Wolfcamp (Midland basin) samples were delivered and prepared for future experiments.

Influence from COVID-19.

Synchrotron beam time for X-ray absorption spectroscopy (XAS) and X-ray fluorescence (XRF) mapping with micro-X-ray near-edge spectroscopy (µ-XANES) originally scheduled for this quarter have been postponed due to the COVID-19 related closure of SSRL. These analyses will resume once SSRL reopens and the canceled beam runs are rescheduled. Experiments using Wolfcamp shale were scheduled to begin

this quarter, but have been postponed due to COVID-19 related lab closure. These samples have been prepared and the reactions will begin once labs reopen.

Results

Shale mineralogical compositions from x-ray diffraction (XRD) measured before and after reaction for the Bone Spring (top and bottom units) and Marcellus (Outcrop and MSEEL) shales are shown in **Tables 3 and 4**, respectively. As discussed in **Quarter 1 Report, 2020**, the acid spearhead is rapidly neutralized by calcite in the rock for all shales. The dissolution of clays (specifically illite) is observable in the Bone Spring Top unit after reaction in the pressurized reactor. After the three-week reaction period, hexahydroborite ($Ca[B(OH)_4]_2{\cdot}2(H_2O)$) is detectable in the Bone Spring Bottom unit, which is likely due to the release of calcium (calcite dissolution due to the acid spearhead) and high borate concentration (0.14 wt%) in the slickwater from the borate containing crosslinker. For the Marcellus Outcrop shale samples after reaction, the calcite and pyrite contents decreased while gypsum increased. This suggests that calcium and sulfur dissolved from calcite and pyrite, respectively, and reprecipitated as calcium sulfate. No new mineral phases were identified in the MSEEL samples.

Table 3 *Shale mineralogical compositions in weight percentage via XRD analysis of Bone Spring samples (Top and Bottom Unit) pre- and post-reaction. Reactor experiments were performed in duplicate. ND denotes non-detectable by XRD.*

	Calcite (%)	Quartz (%)	Illite (%)	Hexahydro-borite (%)
Bone Spring, Top Unit				
Unreacted	84.4%	4.6%	11.0%	ND
Time-Resolved Reactor	84.8%	5.0%	10.2%	ND
Time-Resolved Reactor Duplicate	84.0%	5.0%	11.0%	ND
Pressurized Reactor	94.0%	6.0%	ND	ND
Pressurized Reactor Duplicate	98.1%	1.9%	ND	ND
Bone Spring, Bottom Unit				
Unreacted	99.0%	1.0%	ND	ND
Time-Resolved Reactor	96.8%	ND	ND	3.2%
Time-Resolved Reactor Dupl	96.8%	ND	ND	3.2%
Pressurized Reactor	96.9%	ND	ND	3.1%
Pressurized Reactor Dupl	96.6%	ND	ND	3.4%

Fe XRF maps of the Bone Spring shale samples are shown in **Figures 4 and 5** (top and bottom unit, respectively). Both show that most of the Fe in the unreacted samples is Fe(III) with a few Fe(II) hotspots. After reaction with the hydraulic fracturing fluid, however, very little Fe(II) is detectable. This suggests that, despite being relatively impermeable (< 5 nD), the hydraulic fracturing fluid was able to penetrate the shale and react with the Fe-bearing phases. Planned shale permeability measurements and micro-computed tomography (μ-CT) images will confirm this.

Collaborative Leveraging

Because lab facilities at Stanford have been shut down due to COVID-19, cores were sent to NETL for imaging in Dustin Crandall's laboratory to minimize scheduling issues at Stanford University's facility that we anticipate once the Stanford facility reopens.

Table 4 *Shale mineralogical compositions in weight percentage via XRD analysis of MSEEL and Marcellus Outcrop samples pre- and post-reaction. Reactor experiments were performed in duplicate (dupl). ND denotes non-detectable by XRD*

	Quartz (%)	Calcite (%)	Pyrite (%)	Illite (%)	Clino-chlore (%)	Musco-vite (%)	Gypsum (%)
Marcellus Outcrop							
Unreacted	32.6%	2.3%	15.9%	21.6%	6.0%	21.6%	ND
Time-Resolved Reactor	32.6%	ND	13.7%	24.4%	2.9%	24.5%	1.9%
Time-Resolved Reactor Dupl	30.9%	ND	13.3%	23.3%	3.8%	26.7%	2.0%
Pressurized Reactor	36.2%	ND	14.6%	17.4%	11.8%	16.3%	3.7%
Pressurized Reactor Dupl	32.5%	ND	15.1%	18.9%	12.4%	17.6%	3.5%
MSEEL							
Unreacted	81.7%	18.3%					
Time-Resolved Reactor	97.4%	2.6%					
Time-Resolved Reactor Dupl	97.6%	2.4%					
Pressurized Reactor	77.0%	23.0%					
Pressurized Reactor Dupl	76.5%	23.5%					

Plans for Next Quarter

Office work being completed during the shutdown:

- Finishing analyzing bulk sulfur XAS for Bone Spring (top and bottom), Marcellus Outcrop, and MSEEL ground samples that were collected in Q2.
- Analyze µ-XRF maps for the Marcellus Outcrop and MSEEL ground shale samples that were collected in Q2.
- Draft manuscript of Bone Spring results (Task 2.1.1.7)
- Revise and submit extended abstract for 2020 URTeC Meeting.
- Begin writing 2 manuscripts based on the Pioneer project data for peer-reviewed publication.

Laboratory operations planned to begin when work restrictions are lifted:

- µ-CT analysis by NETL of the reacted cores
- Conduct reactor experiments using Wolfcamp shale
- Perform bulk Fe XAS measurements (contingent on beamtime scheduling)
- Conduct permeability measurements of the shale cores pre- and post-reaction. (contingent on the arrival of the new whole rock gas permeameter)
- Finalize planning of resumption of laboratory operations.
- SEM-EDS imaging of post-reaction Marcellus samples.

Task 2.1.2: Modeling activity

Qingyun Li, SLAC

Task Summary

Numerical modeling of shale matrix alteration is critical for understanding the relationship between geochemical reactions and transport during shale matrix alteration. It allows experiments to be focused on

critical outcome scenarios. Synergy between experiments and modeling has significantly improved the rate of discovery in this project.

To understand the reactivity of shale matrices, in FY 2019, we built an efficient reactive transport model to understand the coupling of transport and chemical reactions in the shale matrices. This model can be adapted to experimental systems in **Task 2.1.1**. To better understand the influence from various factors on shale matrix alteration, we are conducting sensitivity analyses of the reactive transport model. The results from the model sensitivity analyses will tell us which parameters we need to know the best or to control the most efficiently in order to reduce scale mineral formation.

Objectives and Approach

We plan to do both a global sensitivity analysis (which considers variations of all input parameters at the same time) and a local sensitivity analysis (which predicts the influence from one parameter at a time). This will allow us to compare the importance of parameters (such as fluid pH, porosity, aqueous concentrations, etc.) in the overall parameter space versus at a local point. In **FY2020 Q2**, the objective was to establish the workflow for the global sensitivity analysis, including several steps as shown in **Table 5**.

Progress in FY 2020 Quarter 2

The workflow of the global sensitivity analysis was established in **FY2020 Q2**. Selected input parameters such as calcite dissolution rate, diffusion coefficient, and hydraulic fracturing fluid (HFF) pH were varied randomly for each model run, and the corresponding model results were recorded. The model was run for 400 times. The input and output data from these 400 runs were recorded, which allowed us to perform a global sensitivity analysis.

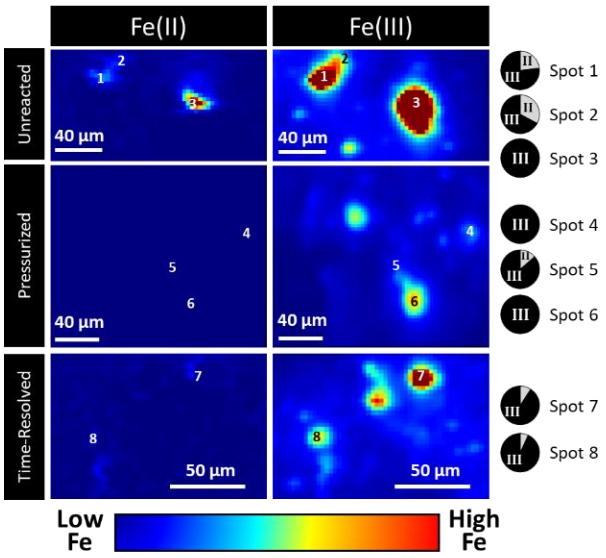

***Figure 5**. Multiple-energy Fe XRF maps of sand-sized shale from Bone Spring Top unit before reaction (**top row**) and after 3 weeks in the pressurized reactor (**middle row**) or the time-resolved reactor (**bottom row**). The color scale, shown at the bottom, is linear and scaled the same for all images. Numbers indicate where µ-XANES were acquired, with the linear combination fits using pyrite and ferrihydrite as Fe(II) and Fe(III) models, respectively, presented as pie charts for each spot.*

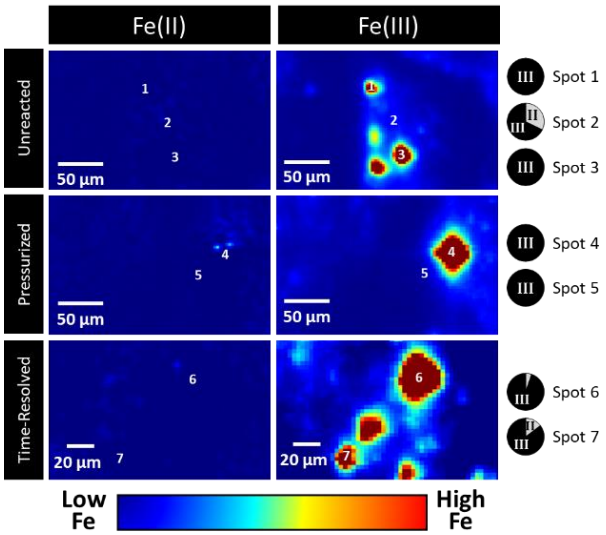

***Figure 4**. Multiple-energy Fe XRF maps of sand-sized shale from Bone Spring Bottom unit before reaction (**top row**) and after 3 weeks in the pressurized reactor (**middle row**) or the time-resolved reactor (**bottom row**). The color scale, shown at the bottom, is linear and scaled the same for all images. Numbers indicate where µ-XANES were acquired, with the linear combination fits using pyrite and ferrihydrite as Fe(II) and Fe(III) models, respectively, presented as pie charts for each spot.*

Table 5 *Task 2.1.2 objectives for* ***FY2020 Q2***

Goal	Status
Automate model parameter selection, model run, and parameter/output recording	Complete
Conduct dimension reduction on selected modeling results	Complete
Conduct global sensitivity analysis using the distance-based generalized sensitivity analysis (DGSA) method[10]	Complete
Interpret the results from global sensitivity analysis	On-going

Influence from COVID-19

Activities under Task 2.1.2 are not affected by COVID-19. The model sensitivity analysis workflow was developed in January and February. Since the shelter-in-place order started in March, we have been following the workflow to collect and analyze data through tele-commuting and online meetings.

Results

Model automation A python script was compiled to automatically select input parameters for the model, run the model, and record the selected results from each model run. At this stage, the parameters being selected are listed in **Table 6**. These input parameters are related to diffusive transport, mineral reactions, aqueous composition, shale composition, aqueous reactions, and finally the calculated parameter from speciation of HFF. Please note that a rate constant is not the rate of the reaction, but is a parameter value that is multiplied to calculate the reaction rate within the model.

The model sensitivity analysis results depend on what results we focus on. For example, the parameters that are most influential for barite precipitation after 21 days of reaction might not be the same parameters that are most influential for porosity alteration after 10 days of reaction. Here, we selected several results to be recorded: (1) pH in each grid cell, (2) porosity in each grid cell, (3) $Fe(OH)_3$ volume fraction in each grid cell, and (4) barite volume fraction in each grid cell, all after 21 days of reaction.

Dimension reduction Because our model has 90 grid cells, one set of results we get from a single run will provide 90 numbers. This means that the results (either porosity, $Fe(OH)_3$ volume, or barite volume) all have 90 dimensions. We found that these 90 dimensions can be reduced to only 2 dimensions (i.e. eigenvectors) using the principle component analysis (PCA) method, with these two dimensions conveying > 85% of the data variation. These two dimensions are purely mathematical constructs that do not translate directly to physical parameters. This dimension reduction step makes the following step on sensitivity analysis more efficient.

Sensitivity analysis The python scripts for model sensitivity analysis using the DGSA method were provided by Prof. Jef Caers' research group (Department of Geological Sciences, Stanford University).[10] The DGSA method uses machine learning strategy to cluster the modeling results (i.e. outputs from our reactive transport model after dimension reduction) into 3 clusters. Results in each cluster have similar features, but these features are different among clusters. The DGSA method then compares the distributions of the input parameters among clusters. For a given input parameters, if its cumulative distribution function is different in each of the three clusters, it means that variation in this parameter in the model input files is related to the different modeling results. In other words, the model is sensitive to this input parameter. Using the DGSA method, **Figure 6** shows the analysis results when we focus on pH, porosity, $Fe(OH)_3$, or barite after

Table 6 *Input parameters for reactive transport modeling which were randomly selected with uniform distribution before each model run.*

	Parameter name	Parameter meaning	Original (based on Marcellus sample)	Range (lower)	Range (upper)	Note
			Transport parameters			
1	m	Cementation exponent	2	0.3	2.3	Related to tortuosity
2	D	Diffusion coefficient	2	1	10	$*10^{-9}$ m^2/s
3	fluid_scale	Factor to scale up/down the original fluid volume	1	0.1	1.5	Fluid grids lengths* fluid_scale
			Mineral reaction rates			
4	O2_s_r	Rate constant for releasing oxidant into fluid	-5.5	-7.5	-3.5	All rate values on shown in log k, where k is the rate constant
5	Pyrite_r	Pyrite reaction rate constant	-7	-9	-5	-
6	Calcite_r	Calcite reaction rate constant	-3.5	-6.5	-0.5	Acid pH pathway
7	Dolomite_r	Dolomite reaction rate constant	-9.5	-11.5	-7.5	Neutral pH pathway
8	Quartz_r	Quartz reaction rate constant	-15	-17	-10	-
9	Illite_r	Illite reaction rate constant	-11	-13	-9	-
10	Barite_rd	Barite reaction rate constant (neutral pH mechanism)	-9.5	-11.5	-7.5	Neutral pH pathway
11	Barite_rh	Barite reaction rate constant (acid pH mechanism)	-8.3	-10.3	-6.3	Acid pH pathway
12	FeOH3_rd	$Fe(OH)_3$ reaction rate constant (neutral pH mechanism)	-13.5	-15.5	-11.5	Neutral pH pathway
13	FeOH3_rh	Fe(OH)3 reaction rate constant (acid pH mechanism)	-8.5	-10.5	-6.5	Acid pH pathway
14	Bitumen_r	Bitumen dissolution rate constant	-2.3	-4.3	-0.3	-
			Water chemistry			
15	pH_fluid	Initial pH in HFF	2	0.5	10	-
16	pH_rock	Initial pH in shale pores	2	0.5	8	-
17	Ba	Ba++ concentration in HFF	0.002	0	0.01	now only vary in HFF not in rock
18	SO4	SO4-- concentration in HFF	0.00006	0	0.0003	now only vary in HFF not in rock
19	Na	Na+ concentration in HFF	0	0	0.5	now only vary in HFF not in rock
20	O2_s_f	Amount of oxidant available	3.8	0	10	$*10^{-6}$,O_2 amount in HFF, not in rock
			Shale composition			
21	Porosity	Shale porosity	0.05	0.005	0.2	Porosity 0.5% - 20%
22	Calcite_f	Calcite fraction in shale	0.01	0	1-por	Depends on porosity
23	Dolomite_f	Dolomite fraction in shale	0.05	0	1-por-cal	Allow total carbonate 90%
24	Pyrite_f	Pyrite fraction in shale	0.055	0	1-por-cal-dol, <0.15	Typical shale has pyrite <15%
25	Illite_f	Illite fraction in shale	0.38	0	1-por-cal-dol-pyr	-
26	Quartz_f	Quartz fraction in shale	0.4	0	1-por-cal-dol-pyr-ill	-
			Aqueous reaction rates			
27	Fe_bit_r	Bitument facilitated Fe++ oxidation rate	5 (7 for Eagle Ford)	4	8	round to digit; rate = $5*10^{'Fe\_bit\_r'}$
			Calculated values			
28	Barite_sat	Barite saturation in HFF	1.3	-	-	Calculated from HFF speciation

21 days of reaction. Values higher than 1 are the influential parameters with 95% confidence level, otherwise the parameters are not statistically influential. Please note that the DGSA method contains stochastic components, so it provides similar but not exactly the same analysis results each time. Therefore, the absolute values for the model input parameters, as well as their sequences, can vary slightly each time when the model analysis scripts are run.

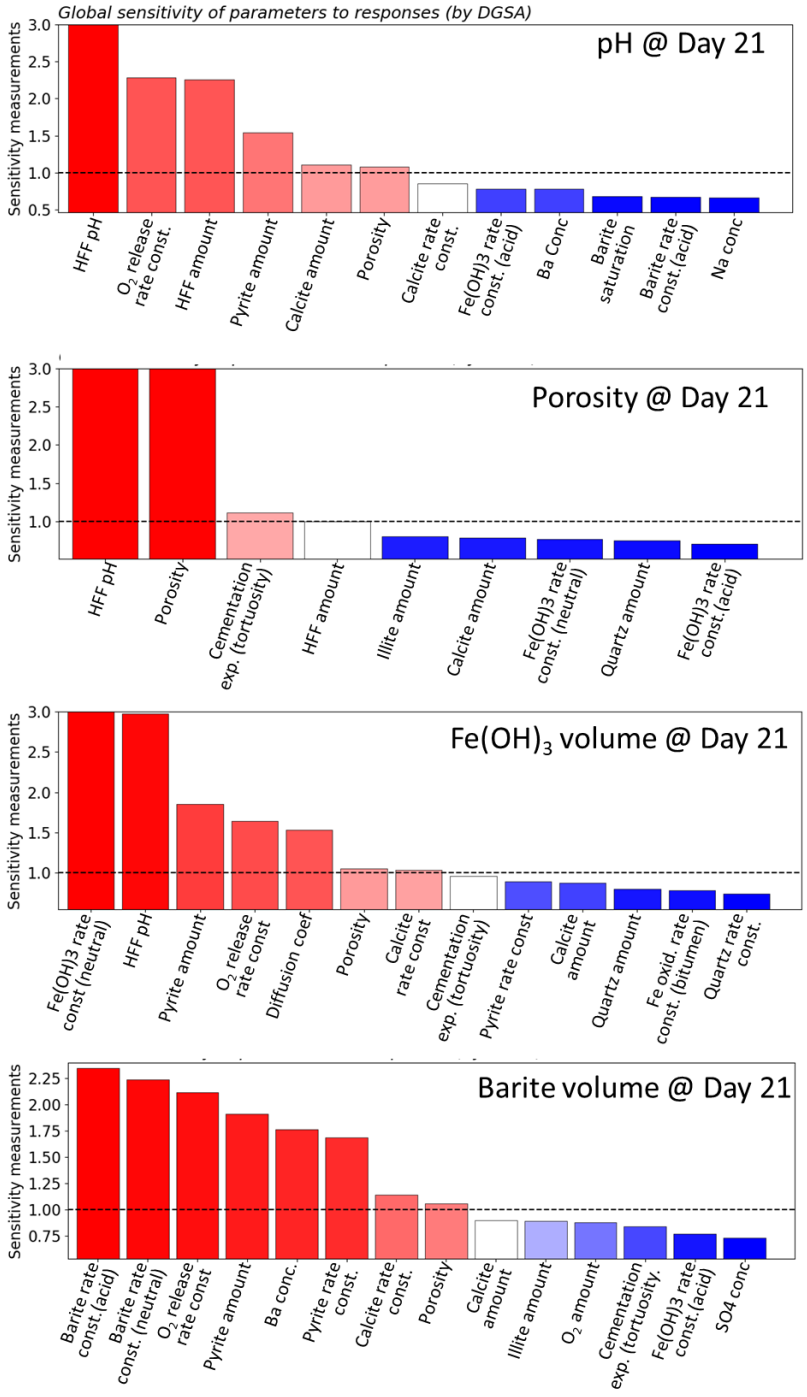

Figure 6*. Global sensitivity analysis results for pH, porosity, $Fe(OH)_3$ formation, and barite formation after 21 days of reaction.*

For pH results at reaction Day 21, **Figure 6** shows that the important input parameters are: The initial pH in the HFF, amount of available HFF, pyrite amount in the shale, and the rate constant for releasing oxidant into HFF. The former two parameters decide the amount of available acid, and the latter two can directly affect pyrite dissolution which feeds back on pH (*i.e.*, creating more acid).

The porosity results at Day 21 are affected mostly by: Original porosity in shale and the initial pH of the HFF. The original porosity affects both the overall porosity level and the rate of acid diffusion through the matrix. The initial pH of the HFF affects the amount of secondary porosity generated from mineral dissolution, especially carbonate dissolution which consumes acid.

The $Fe(OH)_3$ volume at Day 21 is mostly related to: The initial pH of the HFF, the $Fe(OH)_3$ reaction rate constant under near-neutral pH, the pyrite amount in shale, followed by the rate constant for oxidant release, and diffusion coefficient. As stated earlier, the pyrite amount and rate of oxidant release can affect pH. So we can group theses parameters into: pH (including initial pH and factors affecting pH), diffusion, and $Fe(OH)_3$ precipitation rate constant. However, it is interesting to note that although $Fe(OH)_3$ formation is sensitive to pH as expected, not all factors that affect pH are influential for $Fe(OH)_3$ formation. This is the same general observation as for factors that affect pyrite dissolution and diffusion.

The analysis results for barite formation is more complex. **Figure 6** shows that the barite volume results are mostly affected by: Barite rate constants (both acidic and neutral pH mechanisms), the rate constant of oxidant release, pyrite amount in shale, Ba concentration in HFF, and pyrite reaction rate constant. It is easy to understand that barite formation is affected by barite rate constants and Ba concentration. It is less easy to understand the appearance of the rate constant of oxidant release, the pyrite amount, and the pyrite reaction rate. Here are three hypotheses.

First, these parameters affect pH (especially the rate constant of oxidant release and the pyrite amount in shale, as shown in the analysis for pH results), which subsequently affects barite precipitation through both kinetics and thermodynamics. The caveat of this explanation is that the most important factors that affect pH, namely the stimulation fluid pH and amount, do not appear in the analysis for barite formation. We will address this in future work.

Second, the parameters (rate constant of oxidant release, the pyrite amount, and the pyrite reaction rate constant) are important for $Fe(OH)_3$ formation, as stated earlier. It is likely that the conditions that are favorable for $Fe(OH)_3$ formation are also favorable for barite formation. However, at this point, it is not clear what these conditions are, and why the parameters influential for barite formation not showing up as influential parameters for $Fe(OH)_3$ formation. This is another target for resolving in future quarters.

Third, pyrite dissolution can produce sulfate which is one of the reactants for barite precipitation. Parameters that affect pyrite dissolution (rate constant of oxidant release, the pyrite amount, and the pyrite reaction rate constant) can produce sulfate anions, which then promote barite precipitation. To test this hypothesis, we need further analysis of the production and consumption rates of sulfate anions.

Because of the importance of barite formation in affecting permeability, we will continue to study the factors to which barite formation is sensitive.

Deliverables

We have received the reviewers' comment from Energy & Fuels editorial office for Manuscript "Reactive Transport Modeling of Shale-Fluid Interactions after Imbibition of Fracturing Fluids". The manuscript is under revision. The revised manuscript will be submitted in April, 2020.

Plans for Next Quarter

Activities in Task 2.1.2 can continue during the shutdown period. In the next quarter, we plan to:

- Include more input parameters in the global sensitivity analysis (i.e., temperature)
- Explain how pyrite dissolution might affect barite formation
- Conduct local sensitivity analysis of our reactive transport models.

Task 2.2: Mitigation of mineral scaling in unconventional reservoirs

Task 2.2.1: Modeling activity

Q. Li, SLAC

Task Summary

Our experience in **Task 2.1.1** with Wolfcamp-fluid reactions showed that for the Permian Basin, Sr-bearing scale needs to be controlled downhole. This problem will become even more of an issue in the future as operators increasingly rely on Sr-rich cleaned brine in the base fluids for injection. A new integrated set of experiment- modeling activities was initiated to address this problem. Building on knowledge acquired from our initial Wolfcamp-fluid experiments, we have developed a new hypothesis that will provide a central focus for integrated work between **Tasks 2.1** (Prediction of mineral scaling) and **2.2** (Mitigation of mineral scaling).

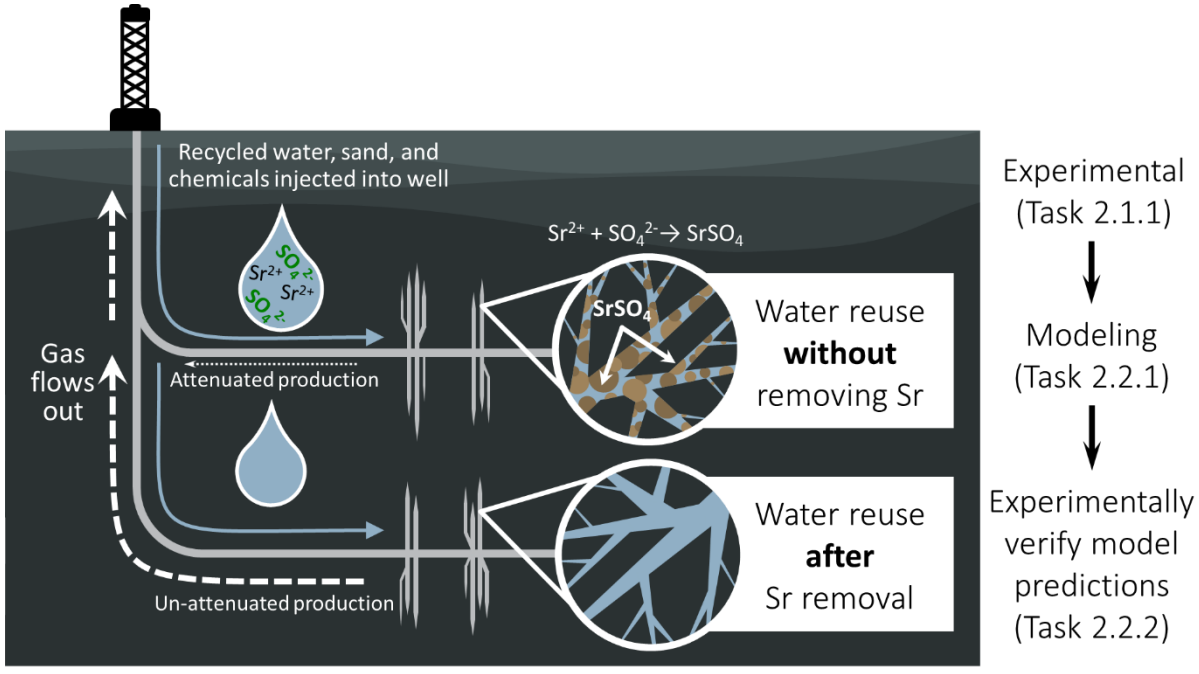

Figure 7*. Conceptual model for mitigation of strontium sulfate scale. Top half: We posit that the presence of abundant dissolved strontium and sulfate causes precipitation and reduced production of hydrocarbons. Bottom half: Removal of strontium from the acid spearhead and stimulation fluid will mitigate strontium scale precipitation and increase production.*

Hypothesis. We posit that removal of primarily Sr from injected brine below a set concentration (to be determined) will mitigate $SrSO_4$ mineral scale precipitation in Wolfcamp shale. This hypothesis is

illustrated in **Figure 7**, where strontium sulfate scales are expected to be largely reduced with a better treatment of the base fluid used to make the fracturing fluid. The significance of this hypothesis is that it allows technology to be brought to focus on mitigating a single solute to achieve the desired performance.

This modeling activity will answer the question: ***How clean does the fracturing fluid need to be in order to mitigate scale mineral formation?*** In order to explore chemical compositions of the fluid to mitigate strontium sulfate scale formation, we will build a numerical model for our Wolfcamp shale sample. Data obtained Wolfcamp shale-fluid reaction experiments (from **Task 2.1.1**) will be used to extract chemical rates using numerical modeling approaches in **Task 2.1.2**. The reaction rates will then be used to predict the amounts of scale minerals where various chemical compositions of the fracturing fluid are assumed (**Task 2.2.1**). The most promising chemical compositions of stimulation fluid proposed based on the modeling work (**Task 2.2.1**) will be evaluated in experimental measurements (**Task 2.2.2**) to confirm its effectiveness in reducing strontium scale minerals.

Influence from COVID-19

Because the modeling work in this task is relied on experimental activities in **Task 2.1.1**, activities in **Task 2.2.1** are expected to be delayed by 3 – 6 months. During SLAC shutdown, we will plan the synergic activities for the experimental and modeling work on Sr scaling management. This planning activity will allow us to proceed efficiently after SLAC re-opens.

Plans for Next Quarter

The task progress is delayed by COVID-19 outbreak because of lab shutdown and communication slow-down under the shelter-in-place order. During the shutdown, we are:

- Conducting planning exercises for the integrated Sr scale subproject to ensure that we are fully prepared to execute it when we are allowed back into the lab in **FY2020 Q3 or Q4**.
- Our goal is to ensure tight connection between modeling activity and experimental measurements.

Task 2.2.2: Experimental activity

Adam Jew, SLAC

Objectives and Approach

As shown with regards to barite scale,[11] this mineral scaling is dominated by multiple components generated across the SRV-well system, and can't be viewed as simple direct alteration of the shale by the injected fracture fluid. In the example of barite scale, the primary constituents (Ba and SO_4) are being introduced to the system by the drillers in the form of drilling mud and the injection of the 15% HCl spearhead. In the Permian Basin, $SrSO_4$ precipitation is a major concern and is derived from the interaction of the base fluid used to make-up the stimulation fluid as well as the shale. Our prior experiments suggest that, if a freshwater base fluid is used, then a portion of the naturally occurring Sr in the rock is leached and the excess Sr, along with Sr in the formation water is brought to the surface. In this situation, Sr scaling downhole is of no concern since Sr and SO_4 concentrations will be lower than the shale in equilibrium with the formation water. But, operators are treating the flowback and produced water for reinjection, the resultant "cleaned" brine is highly elevated in Sr compared to the freshwater counterpart (> 100-fold higher). The use of clean brine causes precipitation of significant quantities of $SrSO_4$ mineral scale on shale surfaces, predominantly in clay-rich members (**Figure 8**). Since scale inhibitors are costly and their efficacy

is marginal, it is important to develop a cost effective and simple process for treating the millions of gallons of clean brine that want to be used for injection.

Table 7 *Task 2.2.2 objectives for FY2020 Q2*

Goal	Status
Reacting Sr-rich clean brine with various $CaSO_4$ mineral species	Complete
Analysis of solutions and solids post-reaction	Ongoing

Progress in FY 2020 Quarter 2

Thermodynamic modeling suggests that adding $CaSO_4$ to brine during pretreatment in the form of either gypsum or anhydrite will lower Sr concentrations in clean brine to concentrations where precipitation of scale in matrix and fractures after injection is likely to be minimal. However, since thermodynamic modeling of solutions with ionic strengths greater than 1M is difficult and sometimes inaccurate, laboratory studies are necessary to confirm or refute the modeling results. Experiments using gypsum and anhydrite at two different concentrations (0.5 g or 1.0 g $CaSO_4$ per 40 mL of solution) were completed. Anhydrite was selected because it is isostructural to $SrSO_4$ and should allow for both greater Sr sorption and epitaxial growth of new $SrSO_4$ from the surface of the anhydrite crystals. Gypsum was also tested due to its high abundance and lower cost than anhydrite. Reactions occurred in borosilicate glass vials during end-over-end mixing at room temperature and pressure for a total of 1 week. These conditions were selected because the purpose of this chemical treatment is to clean the solution in the holding ponds at the surface and not downhole. Experiments were completed and solution samples were properly stored for analysis after the facility shutdown caused by Covid-19.

Influence from COVID-19. Experiments were completed a few days prior to SLAC shutting down laboratory facilities due to Covid-19. The Stanford University environmental measurements laboratory was shut down the same day as SLAC resulting in no analyses of the solutions for Ca and Sr or analysis of the solids to determine whether $SrSO_4$ was forming or if there was significant strain of the $CaSO_4$ crystal lattice indicating Sr incorporation into the gypsum/anhydrite grains.

Results

No Results to report.

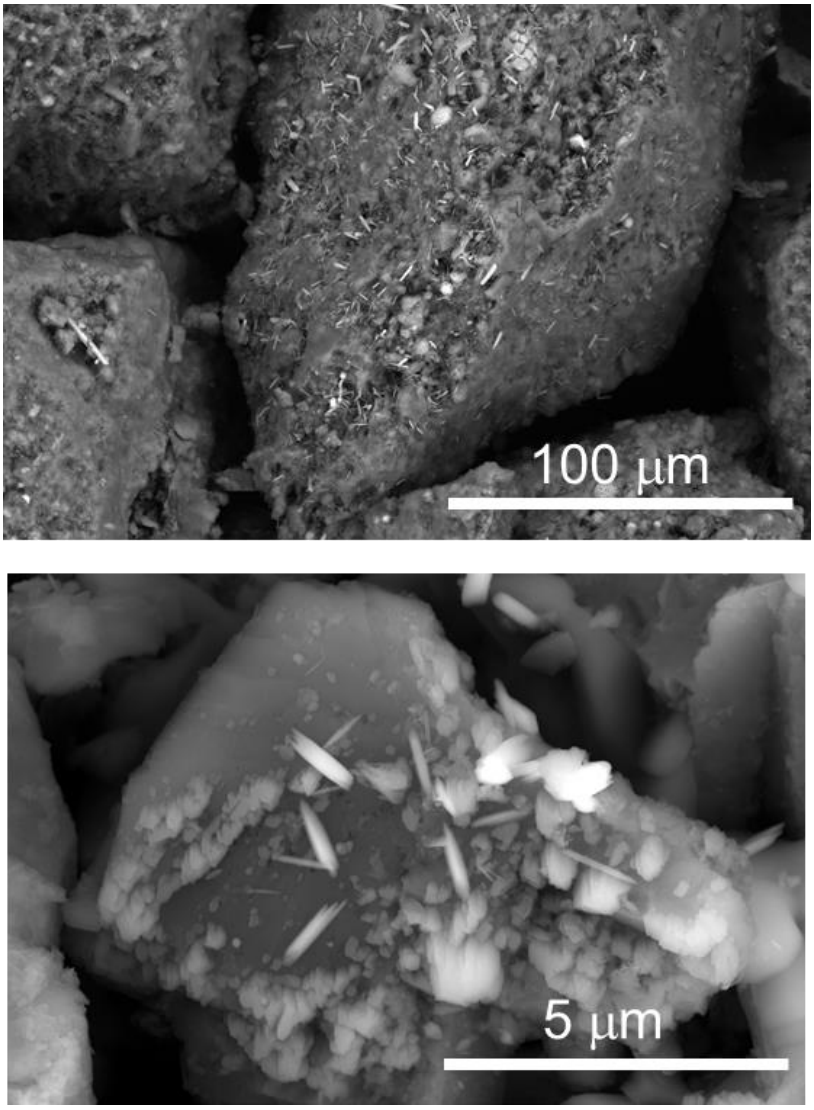

Figure 8. *SEM imaging of clay-rich Wolfcamp shale reacted with hydraulic fracturing fluid comprised of Sr-rich clean brine. Rod shaped crystals on the surface are predominantly $SrSO_4$ with trace amounts of NaCl. XRF analysis of the solids indicates that for clay-rich samples Sr concentrations for shale reacted with clean brine fluids Sr concentrations increase ~5-fold compared to unreacted rock.*

Plans for Next Quarter

- A literature review and development for mitigating Fe(III)-bearing scale mitigation is ongoing. Developing cost-effective measures in order to prevent Fe scale from occurring in the shale matrix is difficult and is requiring extra literature review and thinking. Discussions with the Modeling portion of the project on how to refine the software code in order to handle the high ionic strength (> 1.1 M) as well as speed up calculation time for these labor-intensive calculations is ongoing. This ability will be invaluable as we work towards higher salinity base fluid systems.

Dependent on SLAC and Stanford facilities re-opening:

- Analyze solution samples for Ca and Sr to determine if the treatments with gypsum and anhydrite were successful.

- Do high resolution XRD of solid anhydrite/gypsum used in experiments to determine if Sr incorporated, or precipitating as a new phase. If neither is occurring, we will analyze samples using XAS to determine if Sr adsorption is occurring since XRD can not detect sorbed species
- Additional experiments will be done to determine the lower limit of $CaSO_4$ to solution can be used to have the desired effect. To minimize the cost of this potential treatment, more experiments will be conducted with gypsum-based dry wall to determine its efficacy and potentially have an avenue for reuse instead of sending this waste material to the landfill.

Task 2.3: Acoustic Measurements on laboratory reacted shales

J. Ding, A. C. Clark, and T. Vanorio, Stanford Rock Physics Laboratory

Task Summary

The extremely low permeability of gas shale reservoirs has been requiring hydraulic and acid *fracturing* (*fracking* and *acidification*) for sustained economic productivity. This calls for an enhanced seismic characterization of reservoirs through a rock physics model that includes changes in physical properties due to chemo-mechanical processes. Having a rock physics model that includes rock-fluid interactions provides the basis for monitoring the changes *in situ* through seismic imaging. The evolution of porosity and pore connectivity during geochemical alteration of shales by fracture fluids controls permeability and hence, hydrocarbon production. Acoustic measurements offer the possibility to monitor porosity generation and scale formation in the lab and ultimately in the field (**Figure 9**). However, changes in these properties cannot currently be monitored in the field through seismic imaging because the rock physics employed still rely on purely mechanical models. Since fracture fluid-rock interaction primarily occurs on the created fracture surfaces, it is critical to improve our understanding on the acoustic response that results from the formation of fracture altered zones. We have initiated a set of laboratory-scale experiments to examine the evolution of microstructure, porosity, and ultrasonic velocity following the acidification of artificial shale fractures. This experimental work allows us to build a rock physics model that better informs geochemistry-based strategies taken to optimize permeability within unconventional basins.

Objectives and Approach

The first objective of this task is to evaluate the shale properties (i.e., carbonate/sulfide/clay content, stress-sensitivity, bedding/fractures) that influence porosity creation and/or scale precipitation. Next, we will assess the changes in porosity and acoustic velocity, enabling the interpretation of *in situ* seismic imaging through the calibration of the acoustic response of altered shales in the laboratory. This will be accomplished through the following steps: (1) characterization of the microstructure, porosity, strain, and P- and S- velocities of the pre-reaction sample; (2) exposure of shale samples to specific reactive fluids; (3) re-characterization of the sample to evaluate the effects of dissolution and/or scale precipitation on porosity, permeability, and velocity; and (4) the construction of a rock physics model that incorporates the information from the experiments. Ultimately, the laboratory-calibrated model can be used to interpret seismic data in the field (**Figure 9**).

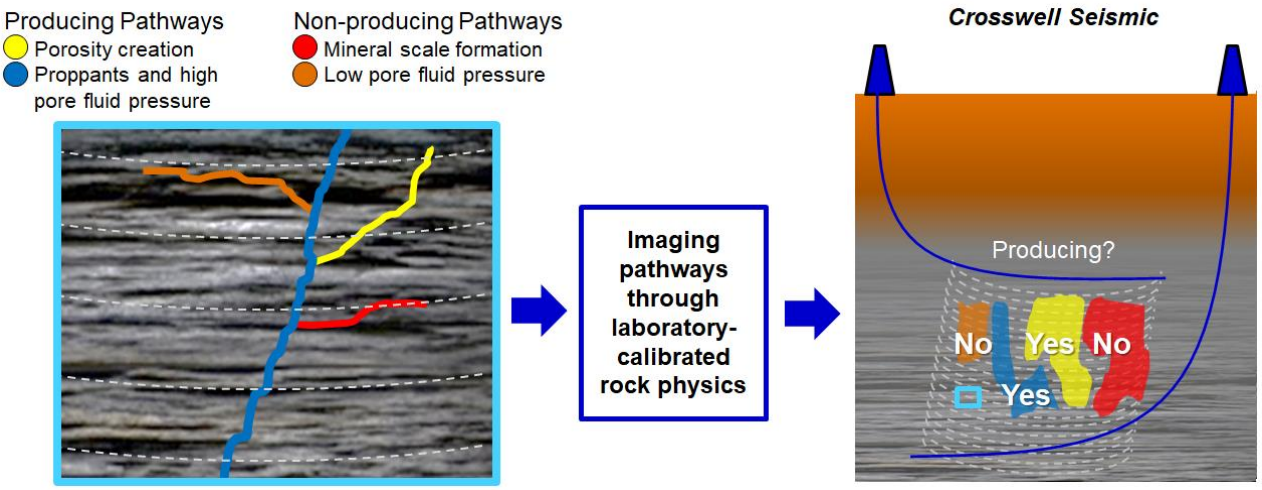

Figure 9. *Conceptual model for Task 2.3. Our approach is to quantify the velocity signatures associated with specific processes that are suspected to exist in the field at the more and microfracture scale (left side). These include: (i) porosity creation, which occurs during acidization of shale reservoirs; (ii) fracture propping; and (iii) application of high pore fluid pressure, which can open microfracture apertures and enhance fluid flow. On the other hand, precipitation of mineral scale clogs pores and microfractures. Pressure management that leads to low pore fluid pressure blocks or closes flow pathways. Manipulating these processes on rock cores under well-controlled conditions in the laboratory and acquiring velocity and permeability data allows for the calibration of a rock physics model, which then can be used to intrepret seismic data acquired in the field in order to identify highly or poorly producing fluid pathways.*

Table 8 Task 2.3 objectives for FY2020 Quarter 2

Goal	Status
React the fractured Marcellus well sample with 15% HCl	Complete
Data analysis of the pre-reaction characterization for the fractured Marcellus well sample	Complete
Characterize the fractured Marcellus well sample after reaction	Complete
Data analysis of the post-reaction characterization for the fractured Marcellus well sample	Ongoing
Prepare and submit SEG and URTeC extended abstracts	Ongoing

Progress in FY2020 Quarter 2

As planned, we finished reacting the fractured Marcellus MSEEL sample with hydrochloric acid (15 v.%) at 7.8 MPa hydrostatic pressure and 80 °C for three weeks. Subsequently, we completed post-reaction characterization of porosity, permeability, acoustic velocity, microstructure, and fracture topography. At the same time, we analyzed all pre-reaction characterization data and post-reaction micro-CT and velocity data. Analysis of post-reaction porosity, permeability and fracture topography is ongoing.

Impacts from COVID-19

The following experiments are delayed due to COVID-19 in Q2:

- ICP-MS analysis of fluid samples from experiments in Q2,
- Experiments on the reacted MSEEL sample upon fracture barite precipitation,
- Experiments on the reacted MSEEL sample upon fracture sand propping.

Results

After reacting the fracture with hydrochloric acid, the clay-rich MSEEL sample developed an altered zone around the fracture that is clearly visible in micro-CT images (**Figure 10**). Comparing images before and after reaction, a darker zone appeared around the fracture, which indicates reduced density. This altered zone extended approximately 1.5 mm into the matrix from fracture surfaces and was a result of dissolution of carbonate and other minerals. In addition to the artificial fracture, this sample contains other microfractures that are sub-parallel to bedding. The acid-resistant epoxy coating on sample exterior surfaces prevented these fractures from being altered, which allowed us to focus on the geochemical effects on the elastic properties of a single fracture.

Fracture acidizing of the clay-rich (and carbonate-poor) Marcellus core had a minor effect on P- and fast S-wave (oscillation parallel to fracture) velocities (**Figure 11**). After the reaction, both P- and fast S-wave velocities at varying confining pressures were unchanged within experimental uncertainty. In contrast, slow S-wave (oscillation perpendicular to fracture) velocities exhibited a measurable reduction ranging from 1.4% to 2.9%. The greater sensitivity of the S-wave is consistent with the findings of Rampton and Hammack (2018),[12] who showed that fracture stimulation in a Marcellus reservoir produced a greater retardation of S-wave velocities than P-waves. Fracture acidizing of this sample with 15 v.% HCl represents an end-member geochemical dissolution scenario for low-carbonate ($\leqslant$5 w.%) Marcellus shale. The results suggest that the slow S-wave velocity (or shear-wave splitting) could be the most useful monitoring tool, given it was the only wave mode among those probed sensitive to geochemical fracture alteration. When traveling parallel to a through-going fracture, the slow S-wave can be viewed as coupled Rayleigh waves propagating along the fracture interface with a velocity that depends on fracture properties (e.g., stiffness), whereas P- and fast S-waves are body waves with velocities insensitive to the fracture.[13]

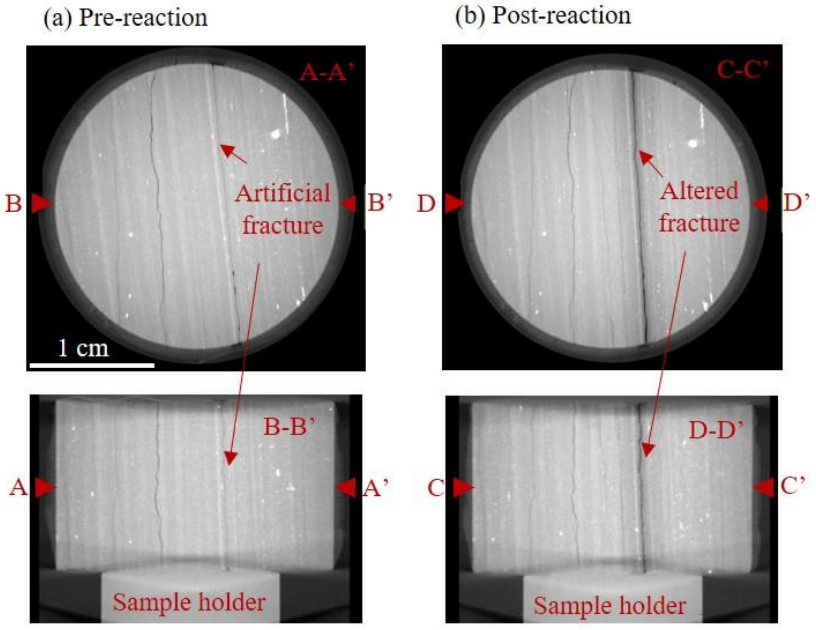

Figure 10*. Micro-CT images of the clay-rich MSEEL sample (a) pre-reaction and (b) post-reaction. The altered fracture is clearly identified as the darker zone around the artificial fracture,which indicates decreased density extending approximately 1.5 mm from each fracture surface. There are other microfractures away from the artificial fracture. These partial microfractures did not react with acid due to the epoxy coating on sample exterior surfaces.*

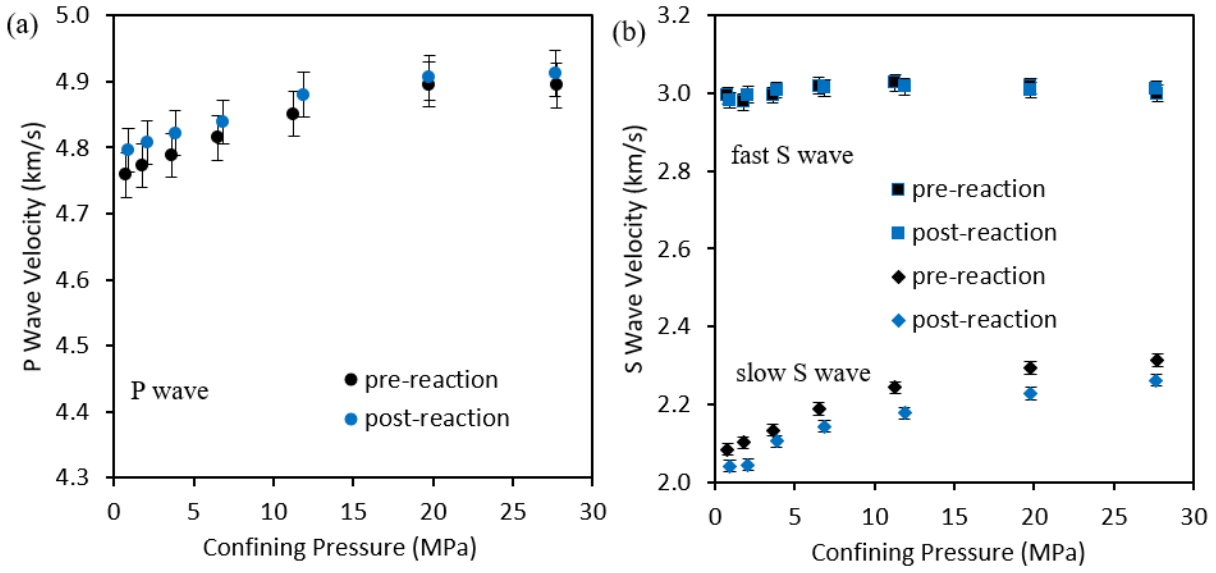

Figure 11. *Pre- and post-reaction (a) P-wave velocity and (b) S-wave velocity of the clay-rich MSEEL sample. The fast and slow S-waves propagate through sample with an oscillation that is, respectively, parallel and perpendicular to fracture. Before and after fracture acidizing, P- and fast S-wave velocities were unchanged, slow S-wave velocities decreased from 1.4% to 2.9%.*

Deliverables

Conference abstracts submitted:

- Time-lapse acoustic monitoring of fracture alteration in Marcellus shale (Jihui Ding, Anthony C. Clark, Tiziana Vanorio, Adam Jew, and John R. Bargar), accepted by 2020 URTeC conference
- Monitoring chemo-mechanical mechanical fracture behavior through engineering geophysics experiments (Jihui Ding, Saied Mighani, Anthony C. Clark, Tiziana Vanorio), accepted by 2020 EAGE conference
- Acoustic velocity signatures of acidized and propped fractures in Marcellus shale (Jihui Ding, Anthony C. Clark, Tiziana Vanorio, Adam Jew, and John R. Bargar), in preparation for 2020 SEG conference

Plans for Next Quarter

Work being completed during the shutdown:

- Finish processing and analyzing porosity and permeability results from post-reaction characterization completed in Q2;
- Finish processing fracture topography data collected in Q2;
- Write, review, and submit extended abstract for 2020 SEG meeting;
- Write, review, and submit extended abstract for 2020 URTeC meeting;
- Conduct planning for resumption of laboratory operations.

Laboratory operations planned to begin when work restrictions are lifted:

- Perform ICP-MS analysis of fluid samples from experiments in Q2;
- Conduct experiments on the reacted MSEEL sample upon fracture barite precipitation;
- Conduct experiments on the reacted MSEEL sample upon fracture sand propping.

Task 3: Manipulation of matrix accessibility

A. Gundogar, SLAC; A.R. Kovscek, Stanford University

Task Summary

The rapid decline in hydrocarbon recovery following hydraulic fracturing of individual wells is related to alteration in shale mineralogy after exposure to reactive fluids that inhibits transport in hydraulic fractures and activated native fractures/microcracks.[3] We primarily focus on revealing the prevalent and transport-related interactions between fractured shale and fracture fluids to enhance access to the large volume of hydrocarbons residing in shale matrices. We make use of representative core-flood experiments and multiscale imaging tools in **Task 3**. Specifically, we investigate the alteration in size, morphology, and connectivity of shale primary and secondary porosity features ranging from core-scale (cm) to micron and nanoscales. The laboratory experiments provide the foundation for scale up to field applications.

Objectives and Approach

The objectives of **Task 3** are to evaluate systematically different stimulation fluid components, experimental practices, and the extent to which they enhance or retard flow in the altered zone. The representative flow-through experiments are important to understand how to control mineral precipitation and dissolution rates and to improve permeability of shales. The insights gained in **Task 3** aid in developing strategies to mitigate scale formation and to maximize flow through shale matrices.

In the hydraulically fractured system illustrated in **Figure 1**, our particular interest is to maintain and improve the permeability of the altered zone of within fracture faces (**Figure 12**). A greater and persistent permeability in the altered zone of the shale matrix provides more efficient leak off of strongly acidic fracture fluid away from the vicinity of fracture networks (**Figure 1b top**) and accordingly a greater volume of oil and gas production from deeper within the shale matrix (unaltered zone in **Figure 1b bottom**) by means of connection of microscale porosity across altered matrices. The stimulated zone may extend through the bulk shale matrix from a few meters to tens of meters depending on transport regimes, formation geomechanics, shale mineralogy, formation fluid, and injected fracture fluid compositions. As reactive fracture fluid travels from the major fractures through the incipient cracks, during the injection and soaking period, a significant decrease usually occurs in porosity and permeability of the reacted zone due to scale reactions such as barite, gypsum, and iron precipitation as well as accumulations of fine clay or other mineral particles especially in the pore throats (**Figure 12**). The reduction in altered zone permeability may have a significant detrimental impact on recovery from the shale matrices with great hydrocarbon potential. Optimized fracture fluid compositions will overcome these negative impacts.

We study the impact of rock-fluid reactions on flow properties of shales by means of three complementary experimental approaches: (i) core-flood experiments of reactive fluids in shales with (ii) multiscale and multi-instrument image analysis and (iii) chemical analysis of the pre- and post-reaction shale rocks and effluents. The representative modeling of coupled fluid flow, transport, and heterogeneous reactions on the shale samples is expected to provide better understanding of the porosity-permeability alterations observed in our experiments. In various simulation cases, the reactive transport regimes are characterized by the ratios of typical rates of reaction versus advection and diffusion - Damkohler (Da) vs Peclet (Pe) numbers. Engineers understand reactive transport as well as the extrapolation of laboratory conditions to field conditions through Pe and Da.

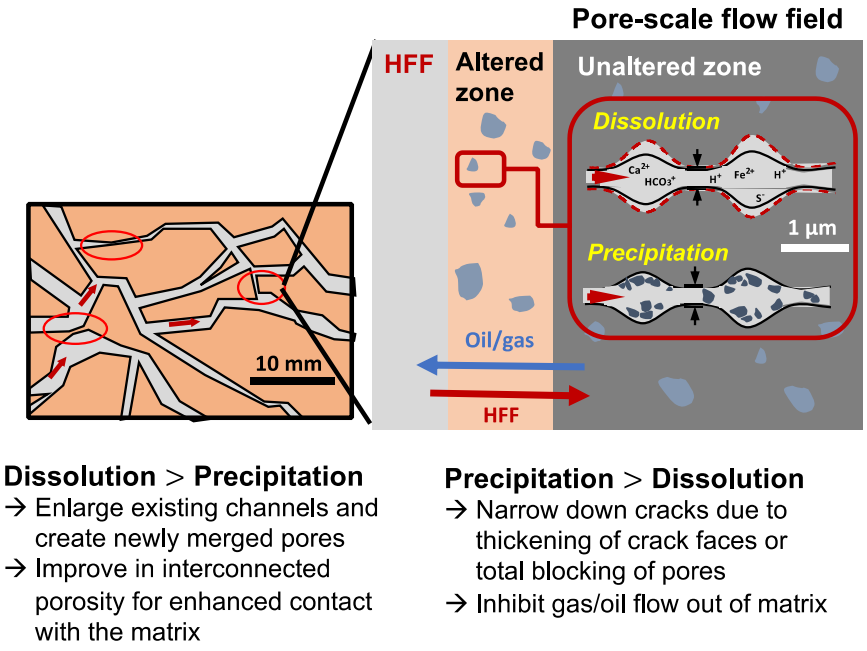

***Figure 12**. Micro to nano-scale pore network system with reactive processes in the "altered zone" induced by HFF exposure. Task 3 is focused on imaging flow and porosity at these scales in order to improve permeability across this important zone.*

***Table 9** Task 3 objectives for FY2020 Q2**

Goal	Status
Perform core-flood experiments	Ongoing
Measure krypton-accessible CT porosities of new pre-/post-reaction shale samples	Ongoing
SEM-EDS analysis of pre- and post-reaction (unpolished) MSEEL calcite-rich sample	Complete
SEM-EDS analysis of reacted Marcellus outcrop, MSEEL calcite-rich samples after polishing	Ongoing
ICP-MS chemical analysis of Marcellus outcrop, MSEEL calcite-rich effluents	Ongoing
Multicomponent reactive transport modeling	Ongoing
Multiscale image processing (2D-3D image registration and segmentation)	Ongoing
Submit the manuscript to 2020 SPE WRM	Complete

* Experimental tasks are awaiting the reopening of laboratories at SLAC and Stanford as discussed in the main text.

Progress in FY2020 Quarter 2

In the last quarter, we completed reactive flow experiments and conducted image analysis for a carbonate-rich (~90 wt% calcite) MSEEL downhole sample. The krypton-accessible CT porosities and their distributions across the core sample were measured before and after reaction. The details of the experimental methodology of gas (Kr) and reactive fluid injection can be found in **FY2019 Q3 and Q4 (annual) reports**. Because we use low flow rates and reactions are slow relative to laboratory time scales, a complete set of core flooding experiments takes longer than 6 weeks to complete (**Figure 10 in FY2020 Q1 report**).

In FY19, NaCl and constant pH HCl solutions were used as models for brine and stimulation fluid for our initial experiments with Marcellus outcrop. In FY20, we are intentionally increasing the chemical complexity of fluids used for the MSEEL calcite-rich sample to better reflect field conditions. The synthetic formation water whose composition was derived from natural Marcellus sources compiled in Warner et al.

(2012) (**Table 10**) and basin-specific HFF mixture modified from the MSEEL recipe in **Appendix C** (excluding guar gum and silica proppant) were used. Subsequently, we explored chemical and structural alterations in matrix and porosity of the carbonate-rich MSEEL sample after reactive fluid exposure are explored by SEM-EDS analysis and CT data.

Table 10 *Saline solution and synthetic formation brine compositions (ppm). Synthetic formation brine is based on the database given in Warner et al. (2012). Abbreviations: Marcellus outcrop (MO), MSEEL carbonate-rich sample (MCB).*

Ion	*Cl*	*Ca*	*Mg*	*Sr*	*Na*	*Ba*
MO	11500	–	–	–	17725	–
MCB	47176	5000	500	1100	22500	2500

Manuscript preparation was a significant task during the last quarter. We submitted an initial manuscript for the SPE (Society of Petroleum Engineers) Western Regional Meeting (WRM) covering our first reactive flow experiments for the clay- and pyrite-rich Marcellus outcrop and carbonate-rich MSEEL samples along with their detailed characterization and image analysis results (note that this submission was earlier than the planned milestone).

Influence from COVID-19: COVID-19 related changes to our work plan may be significant for subsequent quarters of 2020. Our laboratory-based flow experiments with the new samples - clay-rich MSEEL and Eagle Ford shales - and the characterization measurements of pre- and post-reaction cores and effluent analysis are delayed due to the outbreak. There is no access to SNSF (Stanford Nano Shared Facilities) microscopes and microCT scanners. There is limited access to workstations and software products for image processing and elemental analysis. The delay in our laboratory work significantly affects the timing of our milestone items regarding flow experiments, image analysis, and also modeling subtasks. A single core-flood experiment exceeds forty (40) days in duration. Therefore, another three-to-six-month-period (depending on the shelter-in-place duration) is necessary for collecting benchmark experimental data covering different scenarios with different shale mineralogies and fluid compositions for a reasonable sensitivity analysis validated by the real data (Milestone 3.3.2).

Results

During core-flood experiments with the MSEEL carbonate-rich (90 wt% calcite) sample, the average Kr-accessible CT-porosities of the MSEEL carbonate-rich sample before and after reactive fluid injection were found to be 2.5% and 1.7%, respectively. During synthetic formation brine (**Table 10**) injection, the MSEEL carbonate-rich core permeability was 426 µD. After pH 2.0 HCl solution (**Appendix C**) injection, the permeability reduced to 212 µD. Image analysis is used to reveal the changes in shale rock mineralogy causing the resultant reduction in porosity and permeability after interaction with highly acidic HFF.

For SEM imaging, 2.54-cm diameter saw-cut disc surfaces representing the injection surface of the core sample before and after exposure to reactive fluid are used. Discs collected before experiments were polished whereas after the experiment, discs were imaged “as is” and will be polished later. This procedure is followed to capture any surface effects that may be removed by polishing. EDS was used in conjunction with SEM to determine the elemental composition. **Figure 13** shows representative SEM photomicrographs (left) with their EDS spectra (right) of the pre-reaction MSEEL carbonate-rich matrix. In the backscattered SEM images, dark regions represent less dense materials such as organic matter and bright regions correspond to more dense minerals (e.g. pyrite and barite). The dominant elements identified in the pre-reaction sample using EDS affirms the QXRD results (**Table 1 in FY2019 Q4 report**). The mineralogy is mostly calcite and some silicates. In this low porosity sample, the porosity visible in SEM is limited to stylolites and

quartz-rich areas as viewed in **Figure 13**. Stylolites at various scales occur across the core surface. In **Figure 13a**, a stylolite is filled with insoluble components such as clays, pyrite, and organic matter. The clay content is confirmed by the aluminum signal in the EDS spectra. The quartz-rich regions contain visible porosity and minor amounts of clay as shown in **Figure 13b**. Salt (halite) crystals were observed overlying some of the porous quartz-rich regions. These crystals formed while drying the mounts after polishing with fresh water. Authigenic quartz in these regions preserve the porosity by impeding the calcite cementation pervasive in the rest of the sample surface.

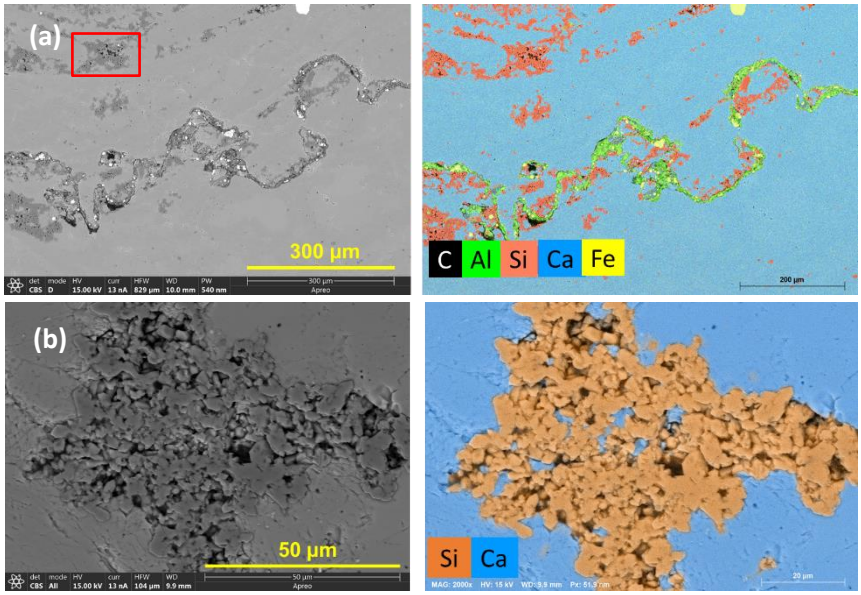

Figure 13 *SEM photomicrographs (left) and EDS composite maps (right) of representative regions in the pre-reaction MSEEL carbonate-rich sample showing both a stylolite and quartz-rich region* ***(a)*** *with a closeup of a porous quartz-rich region* ***(b)****. The high resolution image covering a porous quartz-rich region covered by calcite mineral* ***(b)*** *is out of the field of view of* ***(a)*** *but it stands for similar quartz-rich regions abundant in the low-magnification image one of which is indicated by the red box* ***(a)****.*

Another set of the SEM photomicrographs in **Figure 14** represents the post-reaction carbonate-rich MSEEL sample. The surface of the sample is visibly etched with dissolution surfaces corresponding to cleavage planes in calcite.

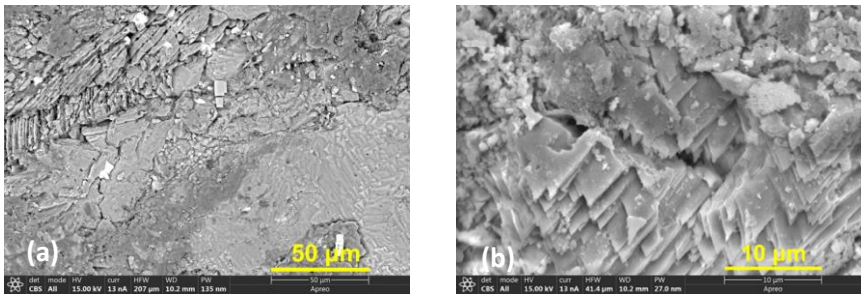

Figure 14 *SEM photomicrographs revealing dissolution textures at different magnifications* ***(a-b)*** *for the post-reaction MSEEL carbonate-rich sample. Dissolution along cleavage planes in calcite is visible.*

Voids and countersunk (dissolved) regions of the reacted core surface contain precipitates (e.g., linear voids in the upper left of **Figure 14a**). Precipitates observed include barite, halite, and hydroxides. Example images in **Figure 15** display some barite ($BaSO_4$) precipitation on the reacted core surface. Particle sizes of barite vary. Barite precipitates are the bright tabular crystals positioned mostly on the lower half of the image in **Figure 15a** and white particles scattered across entire image in **Figure 15b**. The synthetic

formation water composition used for this sample includes barium (**Table 10**). This formulation is based upon natural Marcellus water chemistries (Warner et al., 2012). From QXRD results, the pre-reaction core does not contain barite. Imaging results indicate a significant barite scale growth due to the reaction between formation water, the fracture fluid, and, perhaps, the core sample. Cubic halite crystals are also visible in **Figure 14 (left)** and **Figure 15a-b**. The remaining precipitates in voids and countersunk surfaces are interpreted as hydroxides with different compositions, morphologies, and sizes. Densely bladed or rosette-shaped hydroxide precipitates are encountered at different magnifications (not shown). The smallest and least common precipitates are iron hydroxides. The composition of the other hydroxides is more varied; however, it is typically composed of Al and Mg along with Fe, Cl, and some Ca. Calcite surrounds the regions and may underlie the precipitate contributing to the Ca signal. Silicon is usually absent.

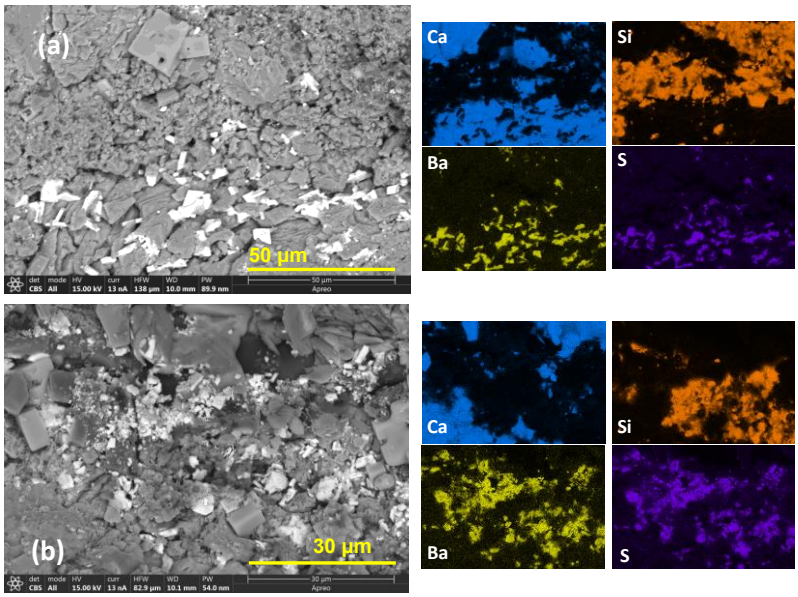

Figure 15 *SEM photomicrographs (left) and EDS elemental maps (right) of barite, and salt precipitates for the post-reaction MSEEL carbonate-rich sample* ***(a, b)****.*

The occurrence of hydroxide precipitates is consistent with the porosity and permeability reduction observed in the core flooding experiments. The hydroxide precipitates have lower densities compared to preexisting calcite and quartz minerals. However, the decrease observed in average CT-number profile suggests preliminarily that the carbonate-rich sample experienced extensive dissolution. The extensive scale precipitation helps to explain the decrease in overall CT-values and accordingly the rock density after HFF injection as given in **Figure 12 of FY2020 Q1 report**. Calcite dissolves readily in acidic HFF and its dissolution results in a decrease in matrix density due to the dissolved minerals. Because these experiments are subject to a confining stress, the core apparently compacted as material was dissolved contributing to reduced porosity and permeability.

Deliverables

Gundogar, A.S.; Ross, C.M.; Li, Q.; Jew, A.D.; Bargar, J.R.; Kovscek, A.R. Multiscale imaging of core flooding experiments during transport of reactive fluids in fractured unconventional shales, 2020 SPE Western Regional Meeting, Bakersfield, CA (Manuscript submitted in March 5, 2020).

Plans for Next Quarter

Work being completed during the shutdown:

- Complete evaluating the core-flooding experimental results obtained in Q2.
- Complete processing (e.g. reconstruction, segmentation, and registration) 3D medical and micro-computed tomography and 2D SEM-EDS image data collected from pre-reaction and post-reaction samples in Q2.
- Review, and elaborate the experimental and image analyses involved in the conference proceeding for 2020 SPE WRM.
- Experimental design and planning for resumption of laboratory operations.
- Progress in developing representative reactive transport model to determine the major chemical and physical parameters controlling the reacted zone flow properties.

Laboratory operations planned to begin when work restrictions are lifted:

- SEM-EDS analysis of the post-reaction Marcellus outcrop and MSEEL carbonate-rich samples after polishing the disk surfaces.
- Chemical analysis of the produced fluid samples collected during HFF injection experiments in Q2 for better understanding of origins and distributions of barite, iron, and other hydroxide precipitates along the core samples.
- Perform reactive flow experiments for clay-rich MSEEL sample.

References

1. Krauss, C., Boom in American Liquefied Natural Gas Is Shaking Up the Energy World. *The New York Times* **2017,** 16.

2. Jew, A. D.; Dustin, M. K.; Harrison, A. L.; Joe-Wong, C. M.; Thomas, D. L.; Maher, K.; Brown Jr, G. E.; Bargar, J. R., Impact of organics and carbonates on the oxidation and precipitation of iron during hydraulic fracturing of shale. *Energy & Fuels* **2017,** 31 (4), 3643-3658.

3. Jew, A.; Harrison, A.; Dustin, M.; Joe-Wong, C.; Thomas, D.; Maher, K.; Brown, G.; Cercone, D.; Bargar, J., Mineralogical and Porosity Alteration Following Fracture Fluid-Shale Reaction. In URTeC: 2017.

4. Cercone, D.; Jew, A. D.; Li, Q.; Dustin, M.; Harrison, A.; Joe-Wong, C.; Thomas, D.; Maher, K.; Brown, G. E., Jr.; Bargar, J. In *Chemical Controls on Secondary Mineral Precipitation of Fe and Ba in Hydraulic Fracturing Systems*, 2017 AIChE Annual Meeting, Minneapolis, MN, Minneapolis, MN.

5. Li, Q.; Jew, A. D.; Kiss, A. M.; Kohli, A.; Alalli, A.; Kovscek, A. R.; Zoback, M. D.; Cercone, D.; Maher, K.; Brown Jr, G. E. In *Imaging Pyrite Oxidation and Barite Precipitation in Gas and Oil Shales*, Unconventional Resources Technology Conference, Houston, Texas, 23-25 July 2018, 2018; 2018; pp 875-884.

6. Liu, Y.; Kan, A.; Zhang, Z.; Yan, C.; Yan, F.; Zhang, F.; Bhandari, N.; Dai, Z.; Ruan, G.; Wang, L., An assay method to determine mineral scale inhibitor efficiency in produced water. *Journal of Petroleum Science and Engineering* **2016,** 143, 103-112.

7. Zhang, F.; Dai, Z.; Yan, C.; Bhandari, N.; Yan, F.; Liu, Y.; Zhang, Z.; Ruan, G.; Kan, A. T.; Tomson, M. B., Barite-Scaling Risk and Inhibition at High Temperature. *SPE Journal* **2017,** 22 (01), 69-79.

8. Shen, D.; Fu, G.; Al-Saiari, H. A.; Kan, A. T.; Tomson, M. B., Barite dissolution/precipitation kinetics in porous media and in the presence and absence of a common scale inhibitor. *SPE Journal* **2009,** 14 (03), 462-471.

9. Li, Q.; Jew, A. D.; Kohli, A.; Maher, K.; Brown Jr, G. E.; Bargar, J. R., Thicknesses of Chemically Altered Zones in Shale Matrices Resulting from Interactions with Hydraulic Fracturing Fluid. *Energy & Fuels* **2019,** 33 (8), 6878-6889.

10. Fenwick, D.; Scheidt, C.; Caers, J., Quantifying asymmetric parameter interactions in sensitivity analysis: application to reservoir modeling. *Mathematical Geosciences* **2014,** 46 (4), 493-511.

11. Jew, A. D.; Li, Q.; Cercone, D.; Maher, K.; Brown Jr, G. E.; Bargar, J. R. In *Barium Sources in Hydraulic Fracturing Systems and Chemical Controls on its Release into Solution*, Unconventional Resources Technology Conference, Houston, Texas, 23-25 July 2018, 2018; 2018; pp 863-874.

12. Rampton, D.; Hammack, R. In *Fracture detection using repeat crosswell seismic in a Marcellus Reservoir*, 2018 SEG International Exposition and Annual Meeting, 2018; Society of Exploration Geophysicists: 2018.

13. Pyrak-Nolte, L. J.; Shao, S.; Abell, B. C., Elastic waves in fractured isotropic and anisotropic media. In *Rock Mechanics and Engineering Volume 1*, CRC Press: 2017; pp 323-361.

Milestone Status

Section	Title	Planned completion date	Revised completion due to COVID-19	Actual completion or status
1.1	Development/Refinement of PMP	7/30/2020	7/30/2020	
1.2	Quarterly research performance reports			
1.3	Meetings with NETL research groups	As Needed	As Needed	
1.4	Annual research performance report			
1.5	Final technical report	9/30/2022	9/30/2022	
Task 2: Scale prediction and mitigation in the stimulated rock volume				
Subtask 2.1: Prediction of mineral scaling in unconventional reservoirs				
2.1.1 Experimental subtask				
2.1.1.1	Evaluate literature/experimental design	3/31/2019	3/31/2019	12/30/18
2.1.1.2	Complete initial scoping experiments	3/31/2019	3/31/2019	2/28/2019
2.1.1.3	React shale with fracture fluid	9/30/2019	9/30/2019	9/30/2019
2.1.1.4	Characterize post-reaction shale samples: laboratory-based methods	12/31/2019	9/30/2020	
2.1.1.5	Analyze solution data from reactor experiments	12/31/2019	12/31/2019	12/31/2019
2.1.1.6	Characterize precipitates: synchrotron-based methods	6/30/2020	12/31/2020	
2.1.1.7	Initial manuscript for subtask 2.1.1	12/31/2020	3/31/2021	
2.1.1.8	Submit manuscript for subtask 2.1.1	3/31/2021	6/30/2021	
2.1.2 Modeling subtask				
2.1.2.1	Develop model framework	6/30/2019	6/30/2019	3/31/2019
2.1.2.2	Test reaction networks against new experimental results from 2.1.1	12/31/2019	12/31/2019	12/31/2019
2.1.2.3	Model parameter sensitivity analysis for major shale system types	3/31/2020	3/31/2020	3/31/2020
2.1.2.4	Reactive transport modeling of systems in 2.1.1	9/30/2020	9/30/2020	12/31/2019
2.1.2.5	Initial manuscript draft for subtask 2.1.2	3/30/2021	3/30/2021	12/31/2019
2.1.2.6	Submit manuscript for subtask 2.1.2	6/30/2021	6/30/2021	12/31/2019
Subtask 2.2: Mitigation of mineral scaling in unconventional reservoirs				
2.2.1 Modeling subtask				
2.2.1.1	Conduct numerical optimization experiments for each shale experiment	6/30/2021	6/30/2021	
2.2.1.2	Evaluate cost/availability of constituents of optimized parameters	12/31/2020	03/31/2021	
2.2.1.3	Develop experimental program based on optimizations	3/31/2021	6/30/2021	
2.2.1.4	Initial manuscript draft for subtasks 2.2.1.1-3	9/30/2021	9/30/2021	
2.2.1.5	Submit manuscript for subtasks 2.2.1.1-3	12/31/2021	12/31/2021	
2.2.1.6	Re-evaluate/refine model as experimental data become available	6/30/2022	6/30/2022	
2.2.1.7	Refine model-based experimental optimization procedure	3/31/2022	3/31/2022	
2.2.1.8	Initial manuscript draft for subtasks 2.2.1.6-7	6/30/2022	6/30/2022	
2.2.1.9	Submit manuscript for subtasks 2.2.1.6-7	9/30/2022	9/30/2022	
2.2.2 Experimental subtask				
2.2.2.1	Formulation of new fracture fluid recipes	5/30/2020	7/30/2020	
2.2.2.2	Testing of new formulations for various scaling conditions	9/30/2020	3/31/2021	
2.2.2.3	React shale with optimized fracture fluid	12/31/2020	6/30/2021	

2.2.2.4	Characterize post-reaction shale samples: laboratory-based methods (optimized fluids)	6/30/2021	12/31/2021	
2.2.2.5	Analyze solution data from reactor experiments (optimized fluids)	6/30/2021	12/31/2021	
2.2.2.6	Characterize precipitates: synchrotron-based methods (optimized fluids)	9/30/2021	12/31/2021	
2.2.2.7	Initial manuscript draft for subtask 2.2.1	12/31/2021	3/31/2022	
2.2.2.8	Submit manuscript draft for subtask 2.2.1	3/30/2022	6/30/2022	
2.2.2.9	Optimize/reformulate fluids	9/30/2021	3/31/2022	
2.2.2.10	Re-test new formulations (after reformulating)	12/31/2021	6/30/2022	
2.2.2.11	Initial manuscript draft for Tasks 2.2.1.9-10	3/31/2022	9/30/2022	
2.2.2.12	Submit manuscript for Tasks 2.2.1.9-10	5/30/2022	12/31/2022	
Subtask 2.3: Acoustic measurements on laboratory reacted shales				
2.3.1	SEM images of top and bottom of unreacted shale	3/31/2019	3/31/2019	3/31/2019
2.3.2	Measurement of grain density, bulk density, and porosity (pre-reacted)	9/30/2019	9/30/2019	9/30/2019
2.3.3	React shale samples with fracture fluid	12/31/2019	12/31/2019	12/31/2019
2.3.4	SEM images of top and bottom of reacted shale	3/31/2020	3/31/2020	3/31/2020
2.3.5	Measurement of grain density, bulk density, and porosity (post-reaction)	9/30/2020	3/31/2021	
2.3.6	Rock physics modeling	12/31/2020	6/30/2021	
2.3.7	Post-injection stress-strain-strength curve measurement	6/30/2022	12/31/2022	
2.3.8	Initial draft of manuscript for Task 2.3	12/31/2021	6/30/2022	
2.3.9	Submit manuscript draft for Task 2.3	3/31/2022	9/30/2022	
Task 3: Manipulation of matrix accessibility ***Subtask 3.1: Manipulate rates of dissolution and precipitation***				
3.1.1	Evaluate literature/experimental design: stimulation conditions	3/31/2019	3/31/2019	3/31/2019
3.1.2	Research/develop stimulation fluid recipes: Marcellus, Midland	3/31/2019	3/31/2019	3/31/2019
3.1.3	Submit synchrotron/neutron user facility proposals	6/30/2019	6/30/2019	6/30/2019
3.1.4	Acquire shale samples	6/30/2019	6/30/2019	6/30/2019
3.1.5	Prepare stimulation fluids	6/30/2019	6/30/2019	6/30/2019
3.1.6	Mineralogical characterization of shale samples	12/31/2019	12/31/2019	12/31/2019
3.1.7	Test reactions: Initial scoping experiments	9/30/2019	9/30/2019	9/30/2019
3.1.8	Evaluate/optimize experiment conditions	9/30/2019	9/30/2019	9/30/2019
3.1.9	Measure permeability of unreacted cores	9/30/2019	9/30/2019	9/30/2019
3.1.10	Collect and process μ-CT images, unreacted cores	12/30/2019	12/30/2019	9/30/2019
3.1.11	Image processing, unreacted cores	3/31/2020	3/31/2020	3/31/2020
3.1.12	Hydrostatic shale core reactions	12/31/2019	12/31/2019	12/31/2019
3.1.13	Collect and process μ-/nano-CT images on reacted cores: macroporosity	12/31/2019	12/31/2019	12/31/2019
3.1.14	SEM characterization: porosity evolution	12/31/2019	12/31/2019	12/31/2019
3.1.15	XRM maps, unreacted/reacted shale cores	9/30/2020	3/31/2021	
3.1.16	Measure permeability of reacted cores	9/30/2020	3/31/2021	
3.1.17	Measure porosimetry of unreacted/reacted cores	3/31/2020	3/31/2020	3/31/2020
3.1.18	Initial manuscript draft for subtask 3.1	12/31/2020	12/31/2020	3/31/2020
3.1.19	Submit manuscript for subtask 3.1	3/31/2021	3/31/2021	3/31/2020
Subtask 3.2: Growth and connectivity of secondary porosity				
3.2.1	Test reactions: Initial scoping experiments	6/30/2020	12/31/2020	
3.2.2	Evaluate/optimize experiment conditions	9/30/2020	3/31/2021	

3.2.3	Pre-characterize samples	9/30/2020	3/31/2021	
3.2.4	React shale samples with fluids	3/31/2021	9/30/2021	
3.2.5	Collect and process μ-/nano-CT images on reacted cores: macroporosity	9/30/2021	3/31/2022	
3.2.6	Image processing, reacted shale cores	12/30/2021	6/30/2022	
3.2.7	2D/SAXS characterization: porosity evolution	9/30/2021	3/31/2022	
3.2.8	SEM (FIB-SEM) characterization: porosity evolution	6/30/2021	12/31/2022	
3.2.9	Initial manuscript draft for subtask 3.2	12/31/2021	6/30/2022	
3.2.10	Submit manuscript for subtask 3.2	3/31/2022	9/30/2022	
Subtask 3.3: Modeling subtask				
3.3.1	Test reaction networks against new experimental data from task 3.1	12/31/2019	12/31/2019	12/31/2019
3.3.2	Model parameter sensitivity analysis for major shale system types	3/31/2020	6/30/2020	
3.3.3	Reactive transport modeling of systems in task 3.1	9/30/2020	9/30/2020	
3.3.4	Initial manuscript draft for subtask 3.2	3/31/2021	3/31/2021	
3.3.5	Submit manuscript for subtask 3.2	6/30/2021	6/30/2021	
Subtask 3.4: Predict and test optimal conditions				
3.4.1	Predict optimal conditions from tasks 3.1, 3.2, 3.3	12/31/2021	6/30/2022	
3.4.2	React shale samples with fluids under optimal conditions	3/31/2022	9/30/2022	
3.4.3	Sample characterization	9/30/2022	Year 5	
3.4.4	Complete initial draft of manuscript for task 3.4	Year 5	Year 5	
3.4.5	Submit manuscript for task 3.4	Year 5	Year 5	

Schedule Status

Task 2.1.1.4 fell behind schedule in FY20 Q2 because the Versa micro-CT instrument that we typically use was out of service due to a failed component between November and February.

Our laboratory operations were suddenly halted by directive from SLAC management on Mar 15, 2020 in response to the growing COVID-19 crisis. Subsequently, on Mar 16, 2020, the county of San Mateo issued an order requiring all residents to shelter in place. This order is still in place at the time of writing. Based on initial discussions at SLAC, we anticipate that laboratory operations may resume as early as July 2020 (an initial estimate), creating a 4-month laboratory schedule slippage. We estimate that another 2 months will be required to process samples already generated (but not yet run) for standard chemical analyses and synchrotron analyses, due to the outstanding backlog and high demand by all users of these shared analytical facilities. The aggregate impact on the project schedule is thus estimated to be about 6 months and is projected in the middle date column above. **The dates in the middle date column are an initial estimate** for long-range planning purposes and **they will be updated in Q3** to reflect additional information that has become available in the interim.

Cost Status

Cost Plan/Status

Basesline Reporting Quarter		Year 7	Start: 10/1/18 End: 9/30/19			Year 8	Start: 10/1/19 End: 9/30/20		
		Q1	Q2	Q3	Q4	Q5	Q6	Q7	Q8
Baseline Cost Plan									
Federal Share	Task 1	$ 28,750	$ 28,750	$ 28,750	$ 28,750	$ 28,750	$ 28,750	$ 28,750	$ 28,750
	Task 2	$ 100,625	$ 100,625	$ 100,625	$ 100,625	$ 100,625	$ 100,625	$ 100,625	$ 100,625
	Task 3	$ 80,500	$ 80,500	$ 80,500	$ 80,500	$ 80,500	$ 80,500	$ 80,500	$ 80,500
	Task 4	$ 77,625	$ 77,625	$ 77,625	$ 77,625	$ 77,625	$ 77,625	$ 77,625	$ 77,625
	Task 5								
	Task 6								
Non-Federal Share									
Total Planned Costs (Federal and Non-Federal)									
Cumulative Baseline Cost		$ 287,500	$ 575,000	$ 862,500	$ 1,150,000	$ 1,437,500	$ 1,725,000	$ 2,012,500	$ 2,300,000
Actual Incurred Costs									
Federal Share	Task 1	$ 6,322	$ 8,227	$ 15,354	$ 34,916	$ 18,430	$ 30,676		
	Task 2	$ 22,127	$ 28,794	$ 53,740	$ 122,207	$ 64,507	$ 107,365		
	Task 3	$ 17,702	$ 23,035	$ 42,992	$ 97,766	$ 51,605	$ 85,892		
	Task 4	$ 17,070	$ 22,213	$ 41,457	$ 94,274	$ 49,762	$ 82,824		
	Task 5	$ -	$ -	$ -	$ -	$ -	$ -	$ -	$ -
	Task 6	$ -	$ -	$ -	$ -	$ -	$ -	$ -	$ -
Non-Federal Share									
Total Incurred Costs - Quarterly (Federal and Non-Federal)									
Cumulative Incurred Cost		$ 63,221	$ 145,490	$ 299,033	$ 648,196	$ 832,501	$ 1,139,257	$ -	$ -
Variance									
Federal Share	Task 1	$ 22,428	$ 20,523	$ 13,396	$ (6,166)	$ 10,320	$ (1,926)	$ 28,750	$ 28,750
	Task 2	$ 78,498	$ 71,831	$ 46,885	$ (21,582)	$ 36,118	$ (6,740)	$ 100,625	$ 100,625
	Task 3	$ 62,798	$ 57,465	$ 37,508	$ (17,266)	$ 28,895	$ (5,392)	$ 80,500	$ 80,500
	Task 4	$ 60,555	$ 55,412	$ 36,168	$ (16,649)	$ 27,863	$ (5,199)	$ 77,625	$ 77,625
	Task 5	$ -	$ -	$ -	$ -	$ -	$ -	$ -	$ -
	Task 6	$ -	$ -	$ -	$ -	$ -	$ -	$ -	$ -
Non-Federal Share		$ -	$ -	$ -	$ -	$ -	$ -	$ -	$ -
Total Variance - Quarterly (Federal and Non-Federal)		$ -	$ -	$ -	$ -	$ -	$ -	$ -	$ -
Cumulative Variance		$ 242,180	$ 447,411	$ 581,368	$ 519,705	$ 622,900	$ 603,644	$ 891,144	$ 1,178,644

Appendix A: Deliverables

Patents.

1. Patent (2019) - Fracture Fluid Alteration to Mitigate Barite Scale Precipitation in Unconventional Oil/Gas Shale Systems. Patent ID: 16/519823

Manuscripts published, submitted, or in revision

2. Jew, A. D.; Bargar, J. R.; Brownlow, J., Strontium behavior in midland basin unconventional reservoirs: the importance of base fluids. *URTeC Extended Abstract*. Accepted and pending revisions, **2020**.
3. Jew, A. D.; Besancon, C. J.; Roycroft, S. J.; Noel, V. S.; Brown, G. E. Jr.; Bargar, J. R., Chemical speciation and stability of uranium in unconventional shales: impact of hydraulic fracture fluid. *Environmental Science and Technology*. Accepted and pending revisions, **2020**.
4. Li, Q.; Jew, A. D.; Brown, G. E. Jr.; Bargar, J. R.; Maher, K., Reactive transport modeling of shale-fluid interactions after imbibition of fracturing fluids. *Energy and Fuels*. In Press, **2020**.
5. Ding, J.; Clark, A. C.; Vanorio, T.; Jew, A. D.; Bargar, J. R., Acoustic velocity signatures of acidized and propped fractures in Marcellus shale. *SEG conference*. Submitted, **2020**.
6. Jew, A. D.; Besancon, C. J.; Roycroft, S. J.; Noel, V. S.; Brown, G. E. Jr.; Bargar, J. R., The effect of hydraulic fracturing fluid on the stability of uranium in unconventional oil/gas shales. *Environmental Science and Technology*. In review, **2020**.
7. Gundogar, A. S.; Ross, C. M.; Li, Q.; Jew, A. D.; Bargar, J. R.; Kovscek, A. R., Multiscale imaging of core flooding experiments during transport of reactive fluids in fractured unconventional shales. *Extended abstract for the 2020 SPE Western Regional Meeting*, *Bakersfield, CA, April 27–30*. Accepted and decided to postpone to a later date, **2020**.
8. Ding, J.; Clark, A. C.; Vanorio, T.; Jew, A. D.; Bargar, J. R., Time-lapse acoustic monitoring of fracture alteration in Marcellus shale. *Extended abstract for 2020 Unconventional Resources Conference, Jul 19-22, 2020, Austin, TX*, **2020**.
9. Ding, J.; Mighani, S.; Clark, A. C.; Vanorio, T., Monitoring chemo-mechanical fracture behavior through engineering geophysics experiments. *Extended abstract for the 82nd EAGE Conference & Exhibition 2020, June 8-11, 2020, Amsterdam, Netherlands*. Accepted and rescheduled to December 10, **2020**.
10. Jew, A. D.; Li, Q.; Cercone, D.; Brown, G.E. Jr.; Bargar, J. R., A new approach to controlling barite scaling in unconventional systems. URTEC-512-MS. *Extended Abstracts of the Unconventional Resources Conference*, **2019**. DOI 10.15530/urtec-2019-512.
11. Li, Q.; Jew, A. D.; Kohli, A.; Maher, K.; Brown, G. E. Jr.; Bargar, J. R., Thicknesses of chemically altered zones in shale matrices resulting from Interactions with hydraulic fracturing fluid. *Energy & Fuels* **2019**, 33 (8), 6878-6889. DOI: 10.1021/acs.energyfuels.8b04527
12. Li, Q.; Jew, A.; Cercone, D.; Bargar, J.; Brown, G. E. Jr.; Maher, K., Geochemical modeling of iron (hydr)oxide scale formation during hydraulic fracturing operations. *SPE/AAPG/SEG Unconventional Resources Technology Conference: Denver, Colorado, USA* **2019**, p 14. DOI: 10.15530/urtec-2019-612.

13. Jew, A. D.; Li, Q.; Cercone, D.; Maher, K.; Brown, G. E. Jr.; Bargar, J. R., Barium sources in hydraulic fracturing systems and chemical controls on its release Into solution. *SPE/AAPG/SEG Unconventional Resources Technology Conference: Houston, Texas, USA* **2018**, p 12. DOI: 10.15530/URTEC-2018-2899671.

14. Li, Q.; Jew, A. D.; Kiss, A. M.; Kohli, A.; Alalli, A.; Kovscek, A. R.; Zoback, M. D.; Cercone, D.; Maher, K.; Brown, G. E., Jr.; Bargar, J. R., Imaging pyrite oxidation and barite precipitation in gas and oil shales. *SPE/AAPG/SEG Unconventional Resources Technology Conference: Houston, Texas, USA* **2018**, p 10. DOI: 10.15530/URTEC-2018-2902747.

15. Alalli, A.; Li, Q.; Jew, A.; Kohli, A.; Bargar, J.; Zoback, M.; Kovscek, A., Effects of hydraulic fracturing fluid chemistry on shale matrix permeability. *SPE/AAPG/SEG Unconventional Resources Technology Conference: Houston, Texas, USA* **2018**, p 10. DOI: 10.15530/URTEC-2018-2881314.

16. Dustin, M. K.; Bargar, J. R.; Jew, A. D.; Harrison, A. L.; Joe-Wong, C.; Thomas, D. L.; Brown, G. E.Jr.; Maher, K., Shale kerogen: hydraulic fracturing fluid interactions and contaminant release. *Energy & Fuels* **2018**, 32 (9), 8966-8977. DOI: 10.1021/acs.energyfuels.8b01037.

17. Jew, A. D.; Harrison, A. L.; Kiss, A. M.; Dustin, M. K.; Joe-Wong, C.; Thomas, D. L.; Maher, K.; Brown, G. E. Jr.; Cercone, D.; Bargar, J. R., Mineralogical and physical changes that control pore-scale shale-gas properties. *SPE/AAPG/SEG Unconventional Resources Technology Conference: Austin, Texas, USA* **2017**, p 7. DOI: 10.15530/urtec-2017-2708858

18. Jew, A. D.; Dustin, M. K.; Harrison, A. L.; Joe-Wong, C. M.; Thomas, D. L.; Maher, K.; Brown, G. E. Jr.; Bargar, J. R., Impact of organics and carbonates on the oxidation and precipitation of iron during hydraulic fracturing of shale. *Energy & Fuels* **2017**, 31 (4), 3643-3658. DOI: 10.1021/acs.energyfuels.6b03220

19. Harrison, A.; Jew, A.; Dustin, M.; Thomas, D.; Joe-Wong, C.; Bargar, J. R.; Johnson, N.; Brown, G. E. Jr.; Maher, K., Element release and reaction-induced porosity alteration during shale-hydraulic fracturing fluid interactions. *Applied Geochemistry* **2017**, 82. DOI: 10.1016/j.apgeochem.2017.05.001

20. Kiss, A.; Jew, A.; Joe-Wong, C.; Maher, K.; Liu, Y.; Brown, G.; Bargar, J., Synchrotron-based transmission x-ray microscopy for improved extraction in shale during hydraulic fracturing. *SPIE: Optical Engineering + Applications*, **2015**; Vol. 9592. DOI: doi:10.1117/12.2190806

Invited Presentations at National Meetings and Departmental Seminars

21. Druhan, J. L.; Ling, B.; Davila, G.; Battiato, I. (2019) Imaging the reactive transport properties of sedimentary formations across scales. Presented at the AGU Fall Meeting. Dec 9-13, San Francisco, CA. [Invited]

22. Noël, V.; Fan, W.; Druhan, J.; Jew, A. D.; Li, Q.; Kovscek, A.; Brown, G. E. Jr.; Bargar, J. R. (2019) X-ray imaging of tracer reactive transport in unconventional shales. Presented at the CMC-UF all hands meeting, Stanford University. Oct 24. Palo Alto, CA. [Invited]

23. Jew, A. D.; Li, Q.; Cercone, D.; Brown, G. E. Jr.; Bargar, J. R. (2019) A New approach to controlling barium scaling in unconventional systems. Presented at the URTeC Workshop. Apr. 22. Pittsburgh, PA. [Invited]

24. Bargar, J. R.; Jew, A. D.; Harrison, A. L.; Kiss, A.; Kohli, A.; Li, Q.; Maher, K.; Brown, G. E. Jr. (2017) Geochemistry of shale-fluid reactions at pore and fracture scales. Presented at the Goldschmidt Geochemistry conference. Aug 16. [Invited]

25. Bargar, J. R.; Kiss, A.; Kohli, A.; Harrison, A. L.; Jew, A. D.; Dustin, M.; Joe-Wong, C.; Maher, K.; Brown, G. E. Jr.; Zoback, M.; Liu, Y.; Cercone, D. (2016) Geochemistry of shale-fluid reactions at pore and fracture scales. Presented at the 252nd American Chemical Society National Meeting. Aug 21. [Invited]

26. Bargar, J. R.; Brown, G. E. Jr.; Dustin, M. K.; Harrison, A. L.; Jew, A. D.; Joe-Wong, C.M.; Maher, K. (2015) Geochemical control of shale fracture and matrix permeability. Presented at the Shales without Scales Workshop. Santa Fe, USA. June 10. [Invited]

27. Bargar, J. R.; Brown, G. E. Jr.; Dustin, M. K.; Harrison, A. L.; Jew, A. D.; Joe-Wong, C.M.; Maher, K. (2015) *Geochemical control of shale fracture and matrix permeability*. Presented at Baker Hughes Incorporated, Tomball, USA, July 14. [Invited]

Talks and Posters Presented at National Meetings.

28. Gundogar, A.S.; Ross, C.M.; Li, Q.; Jew, A.D.; Bargar, J.R.; Kovscek, A.R. (2019) Multiscale imaging characterization of fracture fluid migration and reactive transport in shales. Presented at the AGU Fall Meeting. San Francisco, CA. Dec 9-13. [Poster]

29. Noël, V.; Fan, W.; Bargar, J.R.; Druhan, J.; Jew, A.D.; Li, Q.; Brown, G.E. Jr. (2019) Synchrotron x-ray imaging of reactive transport in unconventional shales. Presented at AGU Fall Meeting, symposium H44B: porous media across scales: from interfacial properties to subsurface processes. San Francisco, CA. Dec 12. [Oral]

30. Li, Q.; Jew, A. D.; Brown G. E. Jr.; Bargar, J. R.; Maher, K. (2019) Reactive transport in shale matrix after fracturing fluid imbibition. Presented at the American Institute of Chemical Engineers (AIChE) Annual Meeting, Orlando, FL. November 10-15. [Oral]

31. Noël, V.; Fan, W.; Bargar, J.R.; Druhan, J.; Jew, A.D.; Li, Q.; Kovscek, A.R; Brown, G. E. Jr. (2019) Synchrotron x-ray imaging of reactive transport in unconventional shales. Presented at the SSRL annual users meeting, Menlo Park, CA. Sept 25. [Poster]

32. Jew, A. D.; Harrison, A.; Li, Q.; Cercone, D. P.; Maher, K.; Bargar, J. R.; Brown, G. E. Jr. (2019) Unconventional mineralogy: interactions of hydraulic fracturing fluids with minerals and organic matter in unconventional and tight oil formations. Presented at the Geological Society of America Annual Meeting. Phoenix, AZ. September 23. [Talk]

33. Li, Q.; Jew, A. D.; Bargar, J. R.; Lopano, C. L.; Hakala, A. J.; Stuckman, M. Y. (2019) Shale-gas-fluid interaction for water and energy. Presented at the ACS National Meeting & Exposition. Orlando, FL. March 31. [Talk]

34. Jew, A. (2018) Pore Scale Control of Gas and Fluid Transport at Shale Matrix-Fracture Interfaces. Presented research at Mastering the subsurface through technology innovation partnerships and collaboration: carbon storage and oil and natural gas technologies review meeting, Pittsburgh, PA, Aug. 13-16, 2018. [Talk]

35. Hakala, A.; Morris, J.; Bargar, J. R.; Birkholzer, J. (2018) Fundamental shale interactions-DOE National Laboratory Research. Presented at the DOE Upstream Workshop. Houston, TX. Feb. 14. [Talk]

36. Jew, A. D.; Cercone, D.; Li, Q.; Dustin, M. K.; Harrison, A. L.; Joe-Wong, C.; Thomas, D. L.; Maher, K.; Brown, G. E. Jr.; Bargar, J. R. (2017) Chemical controls on secondary mineral precipitation of Fe and

Ba in hydraulic fracturing systems. Presented at the American Institute of Chemical Engineers (AIChE) Annual Meeting, Minneapolis, MN. Oct. 29-Nov. 3. [Talk]

37. Li, Q.; Jew, A. D.; Brown, G. E. Jr.; Bargar, J. R. (2017) Chemical reactivity of shale matrixes and the effects of barite scale formation. Presented at the AGU Fall Meeting. New Orleans, LA. Dec. 11-15. [Talk]

38. Jew, A. D.; Dustin, M. K.; Harrison, A. L.; Joe-Wong, C.; Thomas, D. L.; Maher, K.; Brown G. E. Jr.; Bargar J. R. (2016) The Importance of pH, oxygen, and bitumen on the oxidation and precipitation of Fe(III)-(oxy)hydroxides during hydraulic fracturing of oil/gas shales. Presented at the American Geophysical Union Fall Meeting. San Francisco, USA. December 13. [Talk]

39. Bargar, J. R.; Kiss, A.; Kohli, A.; Harrison, A. L.; Jew, A. D.; Lim, J.-H.; Liu, Y.; Maher, K.; Zoback, M.; Brown, G. E. Jr. (2016) Synchrotron X-ray imaging to understand porosity development in shales during exposure to hydraulic fracturing fluid. Presented at the American Geophysical Union Fall Meeting. San Francisco, USA. December 12. [Talk]

40. Harrison, A. L.; Maher, K.; Jew, A. D.; Dustin, M. K.; Kiss, A.; Kohli, A.; Thomas, D. L.; Joe-Wong, C.; Brown G. E. Jr.; Bargar, J. R. (2016) The Impact of Mineralogy on the Geochemical Alteration of Shales During Hydraulic Fracturing Operations. Presented at the American Geophysical Union Fall Meeting. San Francisco, USA. December 13. [Talk]

41. Harrison, A.; Maher, K.; Jew, A.; Dustin, M.; Kiss, A.; Kohli, A.; Thomas, D.; Joe-Wong, C.; Liu, Y.; Lim, J.-H.; Brown, G. E. Jr.; Bargar, J. (2016) Physical and chemical alteration of shales during hydraulic fracturing. Presented at the Goldschmidt Conference, Yokohama, Japan. June 29. [Talk]

42. Dustin, M. K.; Jew, A. D.; Harrison, A. L.; Joe-Wong, C.; Thomas, D. L.; Maher, K.; Brown G. E. Jr.; Bargar, J. R. (2015) Kerogen-hydraulic fracture fluid interactions: reactivity and contaminant release. Presented at the American Geophysical Union Fall Meeting. San Francisco, USA. December 14-18. [Talk]

43. Harrison, A. L.; Jew, A. D.; Dustin, M. K.; Joe-Wong, C.; Thomas, D. L.; Maher, K.; Brown, G. E. Jr.; Bargar, J. R. (2015) A geochemical framework for evaluating shale-hydraulic fracture fluid interactions. Presented at the American Geophysical Union Fall Meeting. San Francisco, USA. December 14-18. [Talk]

44. Jew, A. D.; Joe-Wong, C.; Harrison, A. L.; Thomas, D. L.; Dustin, M. K.; Brown, G. E. Jr.; Maher, K Bargar, J. R. (2015) Iron release and precipitation in hydraulic fracturing systems. Presented at the American Geophysical Union Fall Meeting. San Francisco, USA. December 14-18. [Talk]

45. Joe-Wong, C.; Harrison, A. L.; Thomas, D. L.; Dustin, M. K.; Jew, A. D.; Brown, G. E. Jr.; Maher, K.; Bargar, J. R. (2015) Coupled mineral dissolution and precipitation reactions in shale-hydraulic fracturing fluid systems. Presented at the American Geophysical Union Fall Meeting. San Francisco, USA. December 14-18. [Talk]

46. Harrison, A. L. ; Jew, A. D.; Dustin, M. K.; Joe-Wong, C.; Thomas, D. L.; Maher, K.; Brown, G. E. Jr.; Bargar, J. R. (2015) A geochemical framework for evaluating shale-hydraulic fracture fluid interactions. Presented at the Stanford Center for Secure Carbon Storage Research Seminar. Stanford, USA. October 21. [Talk]

47. Dustin, M. K.; Jew, A. D.; Harrison, A. L.; Joe-Wong, C.; Thomas, D. L.; Maher, K.; Brown, G. E. Jr.; Bargar, J. R. (2015) Kerogen-hydraulic fracture fluid interactions: reactivity and contaminant release. Presented at the Stanford Synchrotron Radiation Lightsource user's meeting. Stanford, USA. Oct 7-9. [Talk]

48. Harrison, A. L.; Jew, A. D.; Dustin, M. K.; Joe-Wong, C.; Thomas, D. L.; Maher, K.; Brown G. E. Jr.; Bargar, J. R. (2015) A geochemical framework for evaluating shale-hydraulic fracture fluid interactions. Presented at the Stanford Synchrotron Radiation Lightsource User's Meeting, Stanford, USA, Oct 7-9. [Talk]

Appendix B: Injection Volumes and Schedule

Injection volumes and injection schedule for a typical injection stage for MSEEL and Midland Basin. Red colored bars are representative of the acid spearhead for each of the wells. The lower volume per stage for Permian Basin is due to the higher number of stages for a single well versus MSEEL (~100 stages/well Permian, ~17 stages/well MSEEL). Cumulative volumes for MSEEL and Midland wells are consistent, ~300,000 gallons. Midland and Delaware Basin injection schedule/volumes are similar.

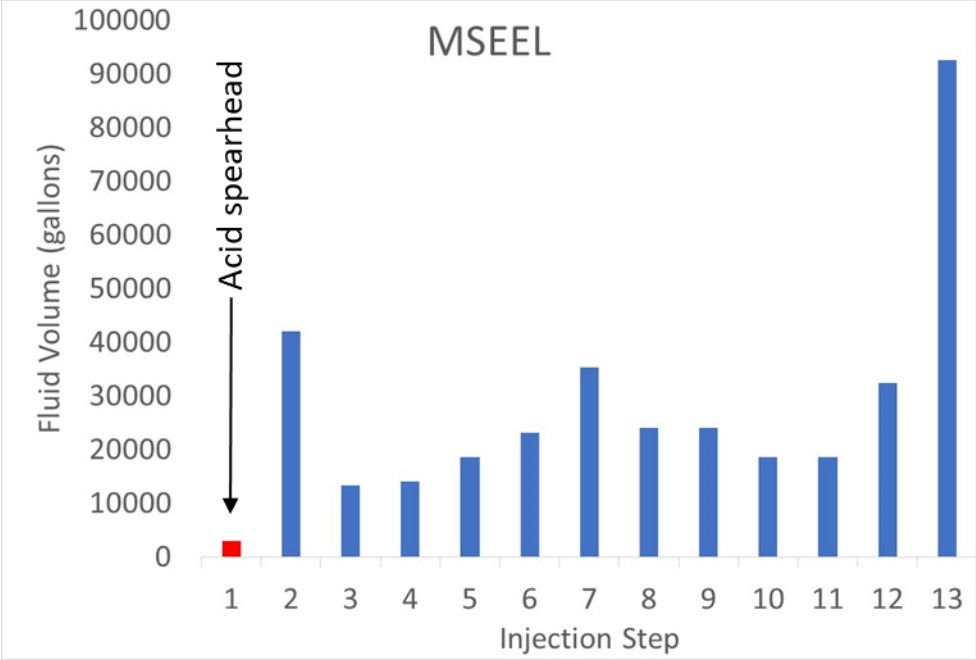

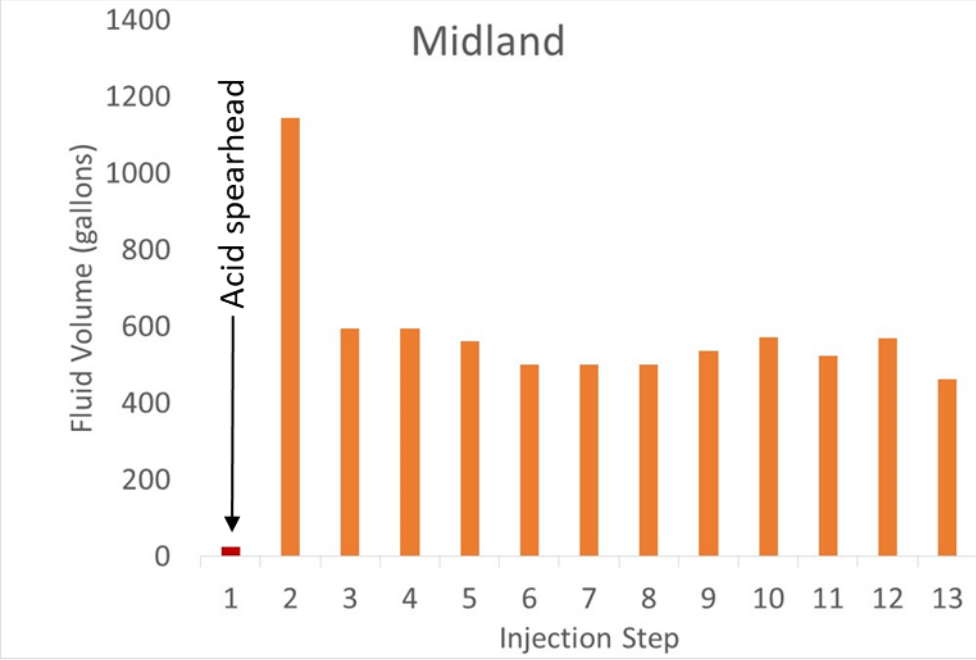

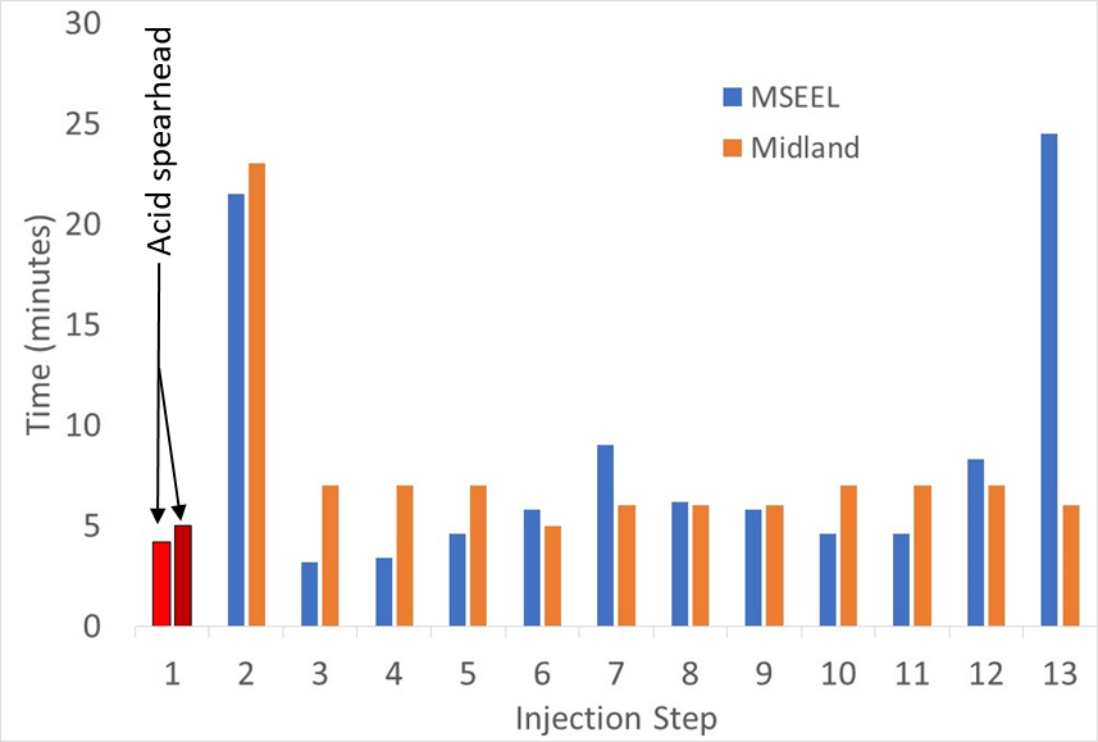
30
25
20
15
10
5
0
Time (minutes)
Acid spearhead
MSEEL
Midland
1
2
3
4
5
6
7
8
9
10
11
12
13
Injection Step

Appendix C: Stimulation Recipes

Stimulation recipes (slickwater) for three different regions Midland, TX (Midland Basin), Reeves Co., TX (Delaware Basin), and MSEEL (Marcellus). Recipes are considered to be average for each area. Chemical concentrations are normalized without silica proppant.

Midland, TX		Reeves Co., TX		MSEEL	
Ingredient	Concentration (% mass) excludes proppant	Ingredient	Concentration (% mass) excludes proppant	Ingredient	Concentration (% mass) excludes proppant
Water	98.30879874	Water	97.10902243	Water	99.70400729
Cupric Chloride	0.000213507	Guar gum	0.17765487	Ammonium sulfate	0.017144809
Thioglycol	0.002314867	Amorphous silica	0.000893534	Acrylamide*	0.012636612
Methyl Alcohol	0.040026969	Glutaraldehyde	0.014138192	Glutaraldehyde	0.0043602
Kerosene	0.202809304	Methanol	0.014138192	Guar gum	0.003130692
C-11 to C-14 alkanes	0.001663108	Ammonium perulfate	0.008743058	Polymer 2-acrylamido-2-methylpropanesulfonic acid	0.001354736
Propylene pentamer	0.052522755	Potassium metaborate	0.135692715		
Methyl Alcohol	0.010506799	Potassium hydroxide	0.013436938		
2-Butoxyethanol	0.030632655	Ethylene glycol	0.013436938	Ethanol 2,2',2"-nitrilotris 1,1',1"-tris(dihydrogen phosphate)	0.001935337
Ammonium Persulfate	0.083425104	Potassium hydroxide	0.010643231		
Gluteraldehyde	0.010473087	2-butoxyethanol	0.020992388		
Methanol	0.006281605	2-propanol	0.020992388	Sodium erythorbate	0.000831056
Polyphosphonic acids	0.006629958	Acetic acid	0.004309321	Urea	0.000831056
Isopropanol	0.006888414	Citric acid	0.002578806	Alkyl(c12-16) dimethylbenzyl ammonium chloride	0.000774135
Propargyl Alcohol	0.006888414	Methanol	0.003766414		
Methanol	0.006888414	Propargyl alcohol	0.000757807		
Isooctyl Alcohol	0.006888414	Ammonium perulfate	0.0085734	Trisodium ortho phospate	0.000580601
Xylene	0.006888414	15% Hydrochloric Acid		Methanol	0.000466758
15% Hydrochloric acid				Fatty acids, Tall-oil	0.000295993
				Thiourea polymer with formaldehyde and 1-phenylethanone	0.000250455
				Sodium sulfate	0.000193534
				Ethylene glycol	0.000170765
				Ethoxylated alcohols	0.000113843
				Ethanol	9.10747E-05
				Propargyl alcohol	7.96903E-05
				2-Propenamid	4.55373E-05
				Hexadec-1-ene	2.27687E-05
				Tetrasodium EDTA	2.27687E-05
				Diammonium peroxidusulphate	1.13843E-05
				1-Octadecene	1.13843E-05
				15 % Hydrochloric Acid	

Appendix D: Recipes for Base Fluids

Recipes for two different base fluids: Monongahela River and Clean Brine. Clean Brine is based on average values measured in Marcellus flowback water minus organics from Paukert Vankeuren, *et al*. (2017). Thermodynamic modeling of Ba and SO_4 concentrations for the Clean Brine indicates that 7% of Ba will precipitate as barite.

ION	FRESH WATER	CLEAN BRINE
	(mM)	(mM)
B^{3+}		0.7
Al^{3+}		0.01
Fe^{3+}		0.02
Ba^{2+}		2
Ca^{2+}	0.3	50
Mg^{2+}	0.4	8.7
Sr^{2+}		5.1
NH_4^+		3
K^+	0.1	2.9
Na^+	1.63	300
SO_4^{2-}	0.7	1.5
NO_3^-	0.05	1
Br^-		1.8
Cl^-	1.5	430
HCO_3^-	3	0.18
pH	7	6

Paukert Vankeuren, A. N.; Hakala, J. A.; Jarvis, K.; Moore, J. E. Mineral Reactions in Shale Gas Reservoirs: Barite Scale Formation from Reusing Produced Water As Hydraulic Fracturing Fluid. *Environ. Sci. Technol.* **2017**, *51* (16), 9391–9402.